ChemElectroChem

Review
doi.org/10.1002/celc.202400065

Chemistry Europe
European Chemical Societies Publishing

www.chemelectrochem.org

Gas Evolution in Li-ion Rechargeable Batteries: A Review on Operando Sensing Technologies, Gassing Mechanisms, and Emerging Trends

Tianye Zheng,*[a, b] Madithedu Muneeswara,[c] Haihong Bao,[a, b] Jiaqiang Huang,[d] Leiting Zhang,[e] David S. Hall,[f] Steven T. Boles,[c, g] and Wei Jin*[a, b]

Gas evolution is fundamentally problematic in rechargeable batteries, and may lead to swelling, smoking, and device-level failure. In laboratories, monitoring gas evolution can help understand dynamic chemical events inside battery cells, such as the formation of solid-electrolyte interphases, structural change of electrodes, and electrolyte degradation reactions. However, gassing in commercial batteries, discrete or continuous, is not monitored due to a lack of compatible sensing technologies. Here we describe the working principles of four real-time gas monitoring technologies for lithium-ion batteries. Gassing mechanisms and reaction pathways of five major gaseous species, namely H_2, C_2H_4, CO, CO_2, and O_2, are comprehensively summarized. Since pertinent progress has been made on the optical fiber-based sensing of strain, pressure, and temperature of various battery cells recently, special emphasis has been given to fiber-based laser spectroscopy for gas detection. The technical details of the fiber-enhanced photothermal spectroscopy are compared with the four gas sensing technologies, and the commercialization possibilities are discussed. Owing to its small size, flexibility, and robustness, fiber-based sensing technology can be compatible with almost all kinds of battery cells, showcasing their great potential in various applications. It is envisioned that gas-event monitoring of rechargeable cells can be unlocked soon by utilizing fiber-based gas spectroscopy.

1. Introduction

In the 21st century, the shift from fossil-based energy supplies to more sustainable ones is inevitable, leading to significant investment and development of energy storage technologies. Rechargeable batteries are favorable amongst policymakers and industrialists, who recognize the relative simplicity of electric vehicles (EVs) and the infrastructure compatibility afforded by electrical connections, as opposed to hydrogen or other fuels. At the current pace, internal combustion engines may be replaced by rechargeable batteries sooner than previously anticipated.[1] Moreover, rechargeable batteries may be one of the few available solutions for resolving the intermittency issues of various renewable energy sources, especially since many parts across the globe still heavily rely on coal burning to generate electricity. However, the safety concerns of widely applying rechargeable batteries should not be neglected.[2] Incidents like smoking, firing, or device-level failures are often seen in day-to-day news. Whereas it is here emphasized that such hazards are minimal for well-made cells, it is important that as new cell chemistries, geometries, and manufacturing processes are introduced, those new batteries must be at least as safe as today's industry best. Various approaches are developed to mitigate the risks, i.e., the probability and consequences, of these unpredictable incidents. For instance, in cylindrical cells that have rigid steel shells, venting designs of the casing are integrated to prevent the internal pressure from unrestricted accumulation, thereby lowering the risk of cell failures. With the powerfulness and increasing popularity of the technology, future rechargeable batteries are anticipated to be smarter and safer in order to better utilize sustainable energy sources. Hence the perspective of Huang et al. is well-founded, in that sensing is the key to battery life and sustainability.[1]

The importance of battery monitoring is well recognized and early efforts can be tracked back more than 100 years, as

[a] Dr. T. Zheng, Dr. H. Bao, Prof. W. Jin
Department of Electrical and Electronic Engineering, The Hong Kong Polytechnic University, Hung Hom, Kowloon, Hong Kong
E-mail: darren.ty.zheng@connect.polyu.hk
wei.jin@polyu.edu.hk

[b] Dr. T. Zheng, Dr. H. Bao, Prof. W. Jin
Photonics Research Institute, The Hong Kong Polytechnic University, Hung Hom, Kowloon, Hong Kong

[c] Dr. M. Muneeswara, Prof. S. T. Boles
Centre for Advances in Reliability and Safety, Hong Kong Science Park, New Territories, Hong Kong

[d] Ass. Prof. J. Huang
Sustainable Energy and Environment Thrust, The Hong Kong University of Science and Technology (Guangzhou), China

[e] Ass. Prof. L. Zhang
Department of Chemistry – Ångström Laboratory, Uppsala University, Uppsala, Sweden

[f] Ass. Prof. D. S. Hall
Department of Energy and Petroleum Engineering, University of Stavanger, Stavanger, Norway

[g] Prof. S. T. Boles
Department of Energy and Process Engineering, Faculty of Engineering, Norwegian University of Science and Technology, Trondheim, Norway

Tianye (Darren) Zheng is a Postdoctoral Fellow at the Hong Kong Polytechnic University, where he received his doctorate in 2021. His early degrees were obtained from Avans University of Applied Sciences and Wageningen University & Research in the Netherlands. During his education, he has conducted research at Delft University of Technology in the Netherlands, the University of Manitoba in Canada, and Karlsruhe Institute of Technology in Germany. Now his research interests cover battery materials, capacitive devices, and the development of optical fiber-based operando gas sensing techniques for rechargeable batteries.

Madithedu Muneeswara currently works at the Centre for Advances in Reliability and Safety (CAiRS) as a Postdoctoral Scholar. He graduated with a B.Sc. and M.Sc. from Sri Venkateswara University in India. He obtained his Ph.D. in chemistry from Indian Institute of Technology Madras in India. His current endeavor employs fiber-optic sensors to provide insight into the mechanical and thermal characteristics of Li-ion batteries.

Haihong Bao received his B.Eng. and M.Eng. degrees from the University of Electronic Science and Technology of China in 2013 and 2016, respectively. He received his Ph.D. degree from the Hong Kong Polytechnic University in 2020. Afterward, he joined the Department of Electrical and Electronic Engineering at Hong Kong Polytechnic University as a Postdoctoral Fellow. Currently, he holds the position of Research Assistant Professor in the same department. His research interests focus on light-matter (gas) interaction in microstructured optical fibers, advanced spectroscopic techniques for ultra-sensitive and selective gas sensing.

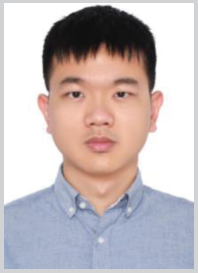

Jiaqiang Huang is an Assistant Professor in Sustainable Energy and Environment Thrust at Hong Kong University of Science and Technology (Guangzhou). He graduated with his Bachelor of Mechanical Engineering degree from Shanghai Jiao Tong University in 2013 and his Ph.D. degree in Mechanical Engineering from the Hong Kong University of Science and Technology in 2017. Afterward, he worked as a postdoc at Hong Kong Polytechnic University and Collège de France with Biao Zhang and Jean-Marie Tarascon, respectively. Dr. Huang's research interests center around batteries, particularly at the interface between novel sensors and new materials/chemistry.

Leiting Zhang is an Assistant Professor at the Department of Chemistry–Ångström Laboratory, Uppsala University, Sweden. He received his degrees from The Hong Kong University of Science and Technology in Hong Kong SAR, China. Dr. Zhang's research team strives to bridge fundamental understandings of battery components, particularly electrodes, electrolytes, and interphases, with technological and methodological breakthroughs in the production and evaluation of high-performance and sustainable batteries. His current research interests include mechanistic understanding of aqueous batteries, development and application of advanced operando characterization techniques, and high-throughput robotic screening of battery chemistries.

David S. Hall is an Associate Professor in Battery Technology at the Department of Energy and Petroleum Engineering. He studied chemistry and materials science at Western University in London, Canada. Dr. Hall is an experienced researcher in the fields of catalysis, corrosion, and electrochemistry. He used to conduct battery research at Dalhousie University in Canada and the University of Cambridge in the UK. His research focuses on the fundamentals and applications of interfacial electrochemistry for sustainable energy storage. His scientific interests are especially related to improving the understanding of physico-chemical processes at electrode-electrolyte interfaces.

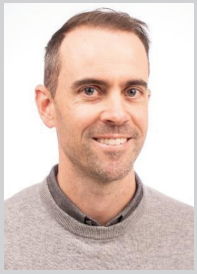

Steven T. Boles is a Professor in Energy and Process Engineering at the Norwegian University of Science and Technology (NTNU) where he has a research focus in Sustainable Energy Systems. He is concurrently a Team Leader at the Centre for Advances in Reliability and Safety (CAiRS) in Hong Kong and maintains an Adjunct Professor position in the Department of Electrical and Electronic Engineering at the Hong Kong Polytechnic University.

Wei Jin currently holds the position of Chair Professor of Photonic Instrumentation in Department of Electrical and Electronic Engineering at the Hong Kong Polytechnic University. He obtained his B.Eng. and M.Sc. from Beijing University of Aeronautics and Astronautics in 1984 and 1987, respectively. He received his Ph.D in Optoelectronics from University of Strathclyde, Scotland, UK, in 1991. Prof. Jin's research interests include photonic crystal fiber devices, optical fiber sensors, fiber lasers and amplifiers, optical gas detectors, condition monitoring of electrical power transformers as well as civil and mechanical structures.

with the ampere-hour meter,[3] pressure transducers,[4] and impedance measurements,[5] all of which were aiming for determination of the state of charge (SoC) and power (SoP), often with secondary benefits towards estimating the state of health (SoH) as accurately as possible. Electrochemical impedance spectroscopy (EIS) works quite well as a purely electrochemical method and is particularly attractive due to its non-destructive nature. Since the invention of electrochemical potentiostats (1940s) and frequency response analyzers (1970s), the EIS technique has been widely used in various electrochemical systems, including rechargeable batteries.[6] Together with other electrochemical post-analysis techniques, such as incremental capacity analysis (ICA), differential voltage analysis (DVA), and intermittent current interruption (ICI), battery performance indicators like SoC, SoP, and SoH can be estimated quite accurately (assuming normal operation). For instance, Bloom et al. have thoroughly developed the theory and applications of DVA.[7] Dahn et al. have developed a freeware based on DVA, of which the parameters are able to provide insights into the mechanisms of cell failure.[8] Such methods are widely adopted and have been further developed by many researchers to identify cell-specific failure modes.[9] Modern battery management systems (BMS) often employ mathematical algorithms and models built upon these electrochemical data for studying battery states.[10] As such, battery monitoring still heavily relies on the interpretation of electrochemical data.

In addition to the methods developed from rich electrochemical data, sensing techniques using independent means are also crucial to probing the internal conditions of various battery products, guaranteeing their reliability and safety during production and operation. For example, the BMS integrated with EVs captures temperature information from the overall battery pack,[11] of which the performance is evaluated together with the electrochemical data, or operational restrictions are put in place. Overheating is considered a vital indicator and a safety concern (e.g., thermal runaway) for batteries in use.[12] Electric sensors, such as thermistors,[13] thermocouples,[14] and resistance temperature detectors,[15] play a critical role in temperature sensing. Acoustic methods were found to be promising in the operando monitoring of energy storage devices. Physical changes in battery cells, such as crack formation and electrode deformation, can be probed by tracking the changes in the sound waves either passively (acoustic emission; AE) or actively (ultrasound testing; UT). Although the technique is simple, low cost, and non-invasive, it is not yet deployed in the commercial field. Environmental interference, such as vibration and noise, would appear as inevitable challenges concerning real applications.[16] Temperature sensors and ultrasound transducers can certainly yield more insights into the internal (electro−) chemistry of batteries. The former has been used to unravel the chemical origins of thermal activities[17] while the latter is suited to capture mechanical changes of solid material or distinguish between the states of matter. Therefore, scientists recognize the value in collecting physical data at the individual cell level, such as temperature,[18] pressure,[19] and strain,[20] to better understand the internal (electro−) chemical, thermal, and mechanical events.

Recently, progress has been made toward harvesting temperature, pressure, and strain data from battery cells.[21] While the gassing issue in batteries is always discussed in these studies, it is seldom discussed independently. In fact, gassing events in batteries are not new and have been acknowledged many times.[1] In commercial battery products, the accumulation of gases may trigger the venting of cylindrical cells or cause swelling of pouch cells. Therefore, external strain variation at a cell-level may partly be caused by the gas evolution inside.[22] This is further supported by the buildup of pressure evidenced by the internal measurement.[17,21a] The production of lithium-ion batteries (LIBs) consists of a formation process, during which the solid-electrolyte interphase (SEI) is deposited on the surface of the negative electrode, usually accompanying evident gas evolution. For pouch cells with soft casing, this amount of gas is often removed after the formation cycles, since the cell can be quickly resealed. One of the most severe incidents in LIB applications, thermal runaway, is also associated with gas release due to exothermic reactions.[12] Noteworthy, these gases are considered the fingerprints of the (electro−) chemical reactions occurring inside battery cells, which is not only scientifically important but could also determine the quality of the battery products. Although the lab-scale operando gas sensing is extended to some large-format cells, it is, by any means, not seen in commercial battery products.[23]

Owing to the inconsistency that gas sensing is considered a crucial component of advanced BMS design and yet is rarely implemented in commercial batteries, e.g., in EVs, this review aims at revisiting currently available gas sensing technologies in laboratories for LIBs, based on which, we share our experiences and comments on the future trends. Firstly, the technical details of four in situ and operando gas sensing technologies, which are available on lab scales, are carefully reviewed. Furthermore, we dive into the details of the gassing mechanisms of five gas species that are often detected and discussed in scientific publications. Afterward, comments are made emphasizing the pros and cons of each technology, shedding light on its potential in academic research and practical applications. Lastly, we summarize this review by considering the application standards, also providing insights into future research that focuses on operando gas sensing techniques for rechargeable batteries and other energy storage devices. Upon successful development of real-time gas sensing in batteries, it is envisioned that various models can be expected based on large sample data. With the help of machine learning and artificial intelligence, the models may be trained to achieve simultaneous assessment as well as incident prediction in future battery products.

2. Available Gas Sensing Technologies for Rechargeable Batteries

Numerous side reactions are occurring in rechargeable batteries during the formation cycle, storage, and operation, which are often accompanied by the generation of gases.[19] Given the complex chemistries inside a battery cell, different gasses could form at different voltages, with different electrolytes, and/or under different working conditions. The importance of gas sensing is well recognized by various research groups, as evidenced by their efforts in developing the experimental apparatus.

2.1. Variable-Volume Gas Syringe Apparatus (VGSA)

Early gas analysis techniques in Li-ion cells can be dated back to 1987,[24] even before Sony introduced the modern LIB products. Fong et al. developed a flange cell with the gas outlet attached to a gas-tight syringe and a differential pressure transducer, which is schematically illustrated in Figure 1. In brief, when the cell undergoes charge-discharge cycles, the gaseous species may evolve and accumulate to result in pressure buildup. Through the pressure regulation by the transducer, the syringe plunger would move and maintain a constant pressure of the dead volume. Quantitatively, the system is able to sense volume changes as low as ± 3 μL.[24]

2.2. The Archimedes' In Situ Gas Analyzer (AISGA)

Several decades later, Aiken et al. of Dahn's group developed an experimental apparatus for the study of gas evolution in pouch cells (flexible casing), namely the Archimedes' in situ gas analyzer (AISGA).[25] As indicated by its name, the apparatus relies on Archimedes' Principle and is schematically illustrated in Figure 2a. The photograph of such a setup is also provided in Figure 2b. When a pouch cell is immersed into a container filled with a fluid, the Buoyant force is well defined as:

$$F_{Buoyant} = \rho g V \tag{1}$$

Where ρ is the density of the fluid, g is the magnitude of gravitational acceleration, and V is the volume of the pouch cell. Once there is gas evolution inside the cell, V would change accordingly, leading to a higher $F_{Buoyant}$ but a nearly constant cell weight (negligible gas weight). Since a hook is introduced for hanging the cell, the force of tension should be introduced, summing up the forces of the system:

$$F_{Sum} = F_{Weight} + F_{Buoyant} + F_{Tension} \tag{2}$$

Based on the theory, Aiken et al. attached the hook to a home-made 'balance', such that the $F_{Tension}$ can be quantified by taking the balance reading via $F_{Tension} = m_{balance} g$. Subsequently, the change of the cell volume, ΔV, can be determined via $\Delta V = \Delta m / \rho$. In the end, a robust testing platform has been established to monitor the volume change of a pouch cell as a function of time.

With this simple yet effective setup, the group then conducted a series of surveys on various commercial Li-ion pouch cells with various chemistries. For instance, Self et al.

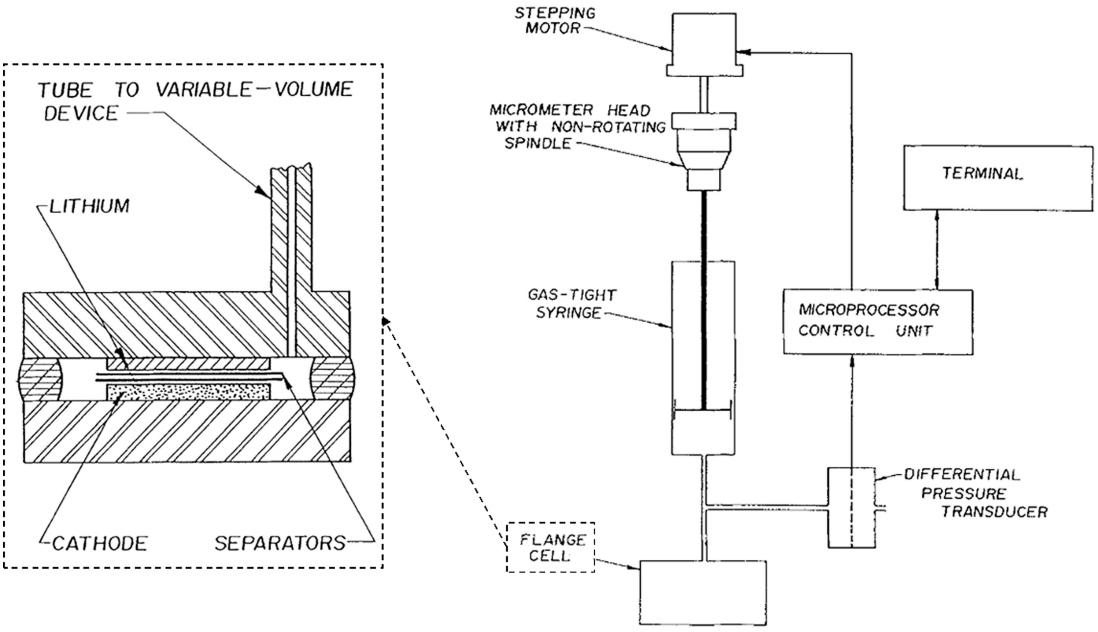

Figure 1. Schematic drawings of the two-electrode flange cell and the constant-pressure gas evolution apparatus used in the gas evolution experiments. Reprinted with permission 1987 IOP Ltd.[24]

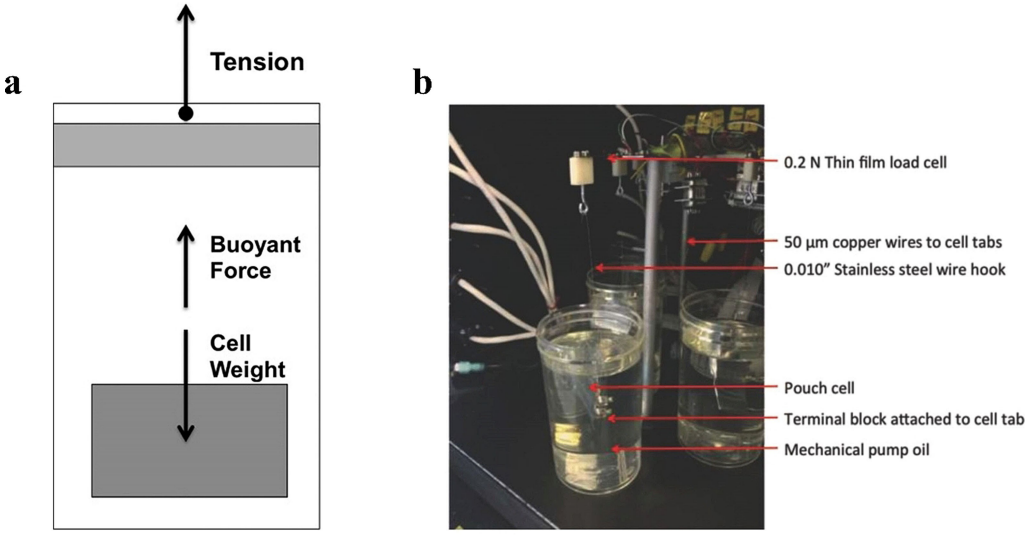

Figure 2. (a) Free body diagram of a pouch cell, prepared with a hole, while hung from a hook. The forces labeled are those present when the cell is hung from a hook and suspended in a fluid. (b) A photograph of the Archimedes In Situ Gas Analyzer (AISGA) with components labeled on one of the five testing channels. Reprinted with permission 2014 IOP Ltd.[25]

investigated the gassing features of the $LiNi_{0.4}Mn_{0.4}Co_{0.2}O_2$ (NMC442) cells with different electrolyte blends and at various temperatures.[26] Meanwhile, Aiken et al. conducted a systematic survey on the influences of electrolyte, electrode material, and temperature on gas evolution in various pouch cells, with extra attention on the formation cycle.[27] It should be noted that the internal chemistries of the testing cells are largely unperturbed using this AISGA setup. This allowed Xiong et al. to explore the interaction between the positive and the negative electrode under various working conditions, suggesting that the gaseous species generated at the cathode may be consumed at the anode.[28] Given the suitability of the AISGA for exploring the gas consumption (i.e., the cells remain properly sealed during the test), Xiong et al. further investigated how the gas generation-consumption affects the electrode impedance.[29] Later Ellis et al. also utilized this platform to quantify and evaluate the effects of gas generation and consumption in NMC/graphite Li-ion pouch cells with conventional carbonate electrolyte solutions. It is found that ca. 60% of the gases evolved during the formation cycle may be consumed after storage for 300 hours.[30]

This Archimedes-based approach can also be used as a routine, ex situ method to measure gas evolution during SEI formation, long-term cycling, high-temperature storage, etc.[31] In this alternative approach, pouch cells are routinely weighed by suspension on a thin wire hook below an analytical balance, while immersed in water. The gas evolution is then calculated from the apparent mass change after whichever test one chooses. In comparison with the AISGA method, this simple ex situ method requires no specialized equipment; although weighing samples on a pan is the method most scientists are familiar with, many analytical balances include a hook on the underside for weighing in this fashion. Moreover, since evaporation over time is not a concern, distilled water may be used as the immersion liquid in place of the silicone pump oil used in the AISGA design. Indeed, ex situ Archimedes' measurements have been an important component of the evaluation of the chemical stability of cell chemistries.[31] Perhaps the best-known example is Harlow et al.'s benchmark study that demonstrated NMC cells may be built to last 'a million miles'.[32]

AISGA measurements can also be coupled with ex situ chemical analysis, in particular, gas chromatography-mass spectrometry (GC-MS),[33] to investigate the chemical mechanisms of the myriad processes in batteries. It is noted that many other studies have employed mass spectrometry to similarly investigate chemical processes, without the direct quantification of the gas volumes produced, and a selection of those reports are discussed later in this article.

2.3. Differential Electrochemical Mass Spectrometry (DEMS)

Imhof and Novák first proposed the differential electrochemical mass spectrometry (DEMS) for battery gas monitoring in 1998, where a gas-permeable barrier (e.g., a membrane) is integrated into a designated cell. When such a cell undergoes cycling, gaseous byproducts can diffuse through this barrier, reaching the mass spectrometer (MS) equipped on the other side. The composition of the gas species can then be analyzed based on their mass-to-charge ratio. In this case, MS signals can be obtained in real-time, allowing for operando monitoring of gas evolution during electrochemical cycling.[34] In the same study, they successfully detected C_2H_4 gas forming on the graphite anode within a specific potential range, shedding light on the decomposition mechanisms of ethylene carbonate (EC) and the formation of SEI. Later in 2005, the same group optimized their DEMS design by introducing an inert gas flow (e.g., helium) to continuously strip out the formed gaseous products. Through such an improvement, they successfully detected a small amount of CO_2 forming on the surface of the graphite anode,

which is believed to come from the decomposition of electrolytes.[35] However, the volatile components, such as dimethyl carbonate (DMC), may be stripped out together with the generated gases, leading to the irreversible loss of electrolytes.[36] Not only does the loss of electrolyte introduce higher background signals in the MS spectra, but it may also lead to electrolyte drying in long-term experiments.

In view of the electrolyte loss in DEMS, Berkes et al. further modified the design by adding a cold trap to condense the vaporized solvents from the electrolyte before the gaseous species approach the MS (Figure 3), such that a higher signal-to-noise ratio can be achieved in the obtained MS spectra.[37] An optional 'humidifier', which is filled with the electrolyte solvent, can also be added to prevent complete dry-out of the cell when long-term experiments are needed. Using this improved DEMS design, more than 100 hours of operando gas monitoring in battery cells is achieved.[22] Nevertheless, an immediate response can hardly be achieved, regardless of how the system is being optimized, and a signal delay of about 30 seconds is inevitable owing to the long gas diffusion path. The other drawback is that some generated gases may be (partly) consumed via engagement in secondary reactions, such as SEI formation,[36] which cannot be captured by DEMS since the gases have already been stripped out. Overall, although the DEMS technique can indeed generate valuable data, the continues sampling nature may make the battery cells deviate from the actual working conditions.

2.4. On-line Electrochemical Mass Spectrometry (OEMS)

To mitigate the issues mentioned in DEMS, alternatively, Tsiuvaras et al. developed the On-line Electrochemical Mass Spectrometry (OEMS), which shares similar working principles as DEMS (Figure 4).[38] While the carrier gas is intentionally removed, a capillary leak is made on the battery cell with a fixed headspace, such that an extra slow gas flow rate can be reached and maintained, e.g., 1 $\mu L\,min^{-1}$. This sampling method is well-aligned with the high-precision MS, which does not necessitate a large sample size, but it could be problematic for other measuring facilities, such as gas chromatography (GC) or absorption spectroscopy. This OEMS platform allows *operando*

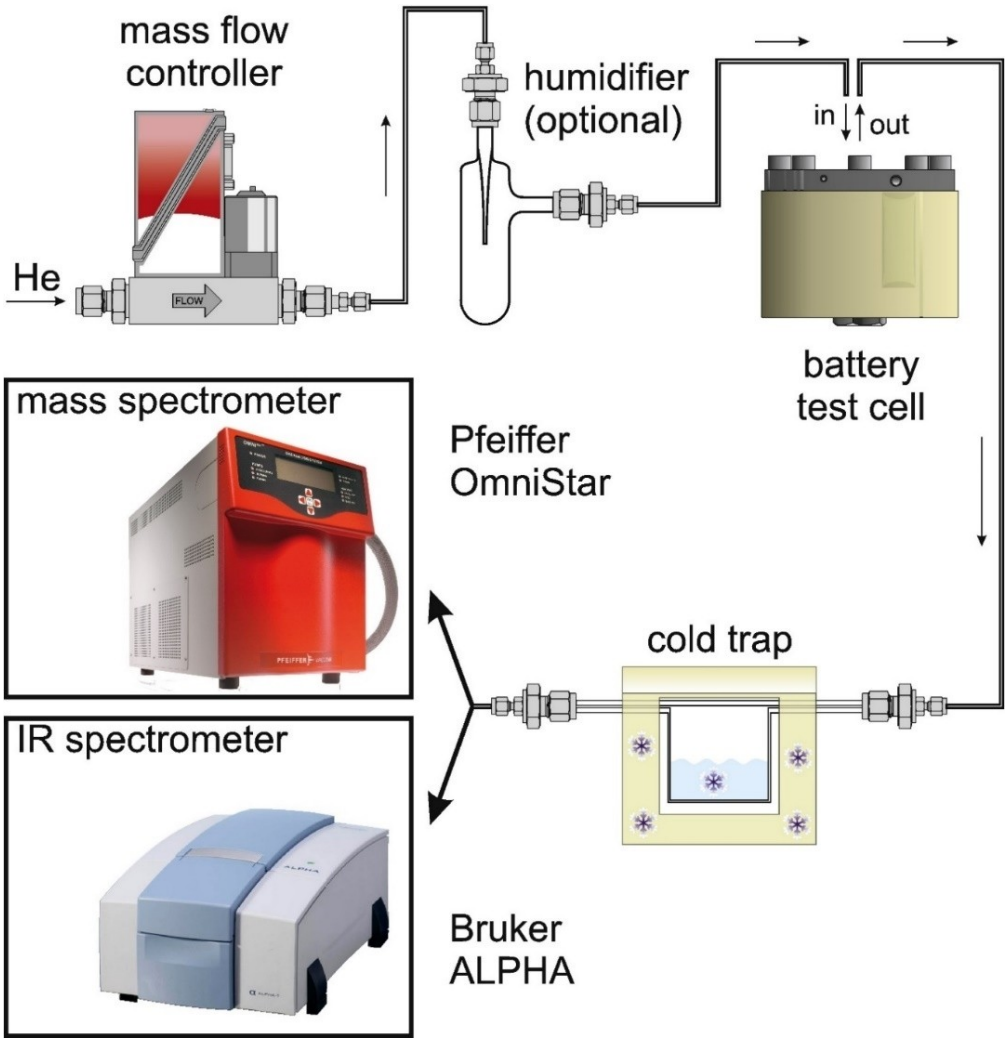

Figure 3. Schematic diagram showing the construction of the DEMS-DEIRS system. Reprinted with permission 2015 Elsevier B.V.[37]

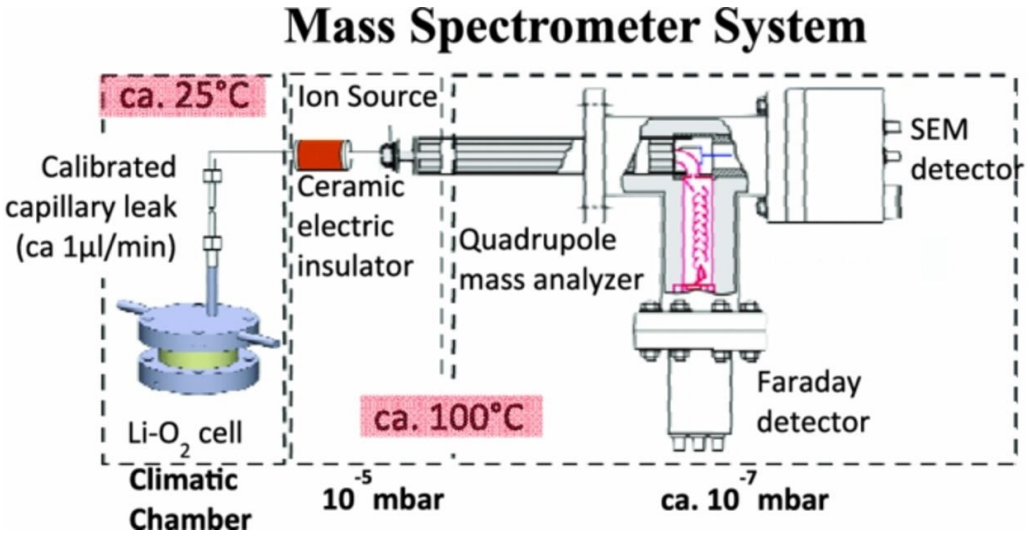

Figure 4. On-line electrochemical mass spectrometer (OEMS) system with a Li-O_2 battery cell (internal gas head space of 9 mL) connected directly through a calibrated crimped-capillary leak (≈1 µL/min) to a mass spectrometer with a closed ionization cage at a pressure of $\approx 10^{-6}$ mbar. All gas products evolved in the battery cell are continuously sampled. Reprinted with permission 2013 IOP Ltd.[38]

monitoring of the dynamic formation of O_2 and CO_2 in Li-O_2 batteries with propylene carbonate (PC) and diglyme electrolytes. Bernhard et al. applied the OEMS technique to LIB cells with different anodes, such as $Li_4Ti_5O_{12}$[39] and graphite.[40] They found that four gasses, namely H_2, C_2H_4, CO, and CO_2, are largely responsible for the electrochemical performance variations. In the meantime, with the well-established OEMS system, a new two-compartment cell was developed and used to quantify the CO_2 evolution from either the carbonaceous materials (e.g., conductive agent; ^{12}C-labelled) or the electrolyte solvent (e.g., EC; ^{13}C-labelled) via anodic oxidation.[41] A similar study was also conducted by Metzger et al. to investigate the H_2 evolution, suggesting that the reduction of H_2O should play a primary role.[42] Later Jung et al. and Streich et al. independently conducted a series of works on the (Li-rich) layered-oxide cathode, focusing on characterizing the possible O_2 release from its lattice during cycling.[43] On the down side, the capillary leak, which releases the gases at a constant rate, the gas pressure inside the battery can hardly be constant. Although it was reported that the OEMS platform only allows an experiment period of typically less than 48 hours, a modified semi-closed OEMS setup designed by Lundström and Berg successfully mitigated the existing issues and extended the measurement time to weeks.[19]

3. Gas Evolution Mechanisms in Li-ion Batteries

The gaseous species formed in LIBs are reported to be correlated with deleterious chemical processes that, in turn, correlate with battery degradation. It is important to note that such correlations are not necessarily well understood or so obviously causal, such as how gas evolution is linked to particle cracking,[44] surface contamination/defects,[45] and the reactivity of surface oxygen moieties at the electrode-electrolyte interface.[46] Among them, the evolution of inorganic species including H_2, CO, and CO_2 are reported to be problematic.[47] Owing to the presence of organic carbonate solvents in electrolyte solutions, many hydrocarbon species can evolve as well, particularly CH_4, C_2H_4, and C_2H_6, of which C_2H_4 is found to be the second-most generated gas in NMC-graphite cells.[30,34] As a result, this section focuses on discussing the four major gases that are frequently detected in all kinds of LIB cells, namely H_2, C_2H_4, CO, and CO_2. In addition, O_2 evolution, which is likely released from the cathode lattice, will be discussed separately together with the cells containing (Li-rich) NMC cathodes.[43a]

3.1. H_2 Evolution in Li-ion Batteries

As a potential byproduct, H_2 can be quite dangerous due to its wide range of flammability (4–74%) and explosion limits (18.3–59.3%) in air.[48] Generally, the evolution of H_2 gas in LIBs is reported to originate from the reduction of residual moisture during the initial formation cycle, supported by reports of LCO//Graphite cells that were prepared with the intentional addition of up to 2,000 ppm H_2O.[49] In this case, the H_2 may be removed from the cell in the controlled environment. Whereas the whole LIB cell manufacturing process is universally accepted to be very sensitive to moisture, e.g., the requirement for dry room and anhydrous electrolyte, the literature suggests that a more nuanced understanding is merited. For instance, water contents higher than 2,000 ppm and 1,000 ppm can negatively affect the cycling performance of LCO//LTO[50] and the LCO//Graphite cells,[51] respectively, in apparent contradiction to Xiong et al.[49] In contrast, Hoffman et al. found that electrolyte solvent reactions with the LTO surface are greater gas creators than dissolved water.[52] Recent studies suggest the more negative effects of ambient water are to accelerate the decomposition of

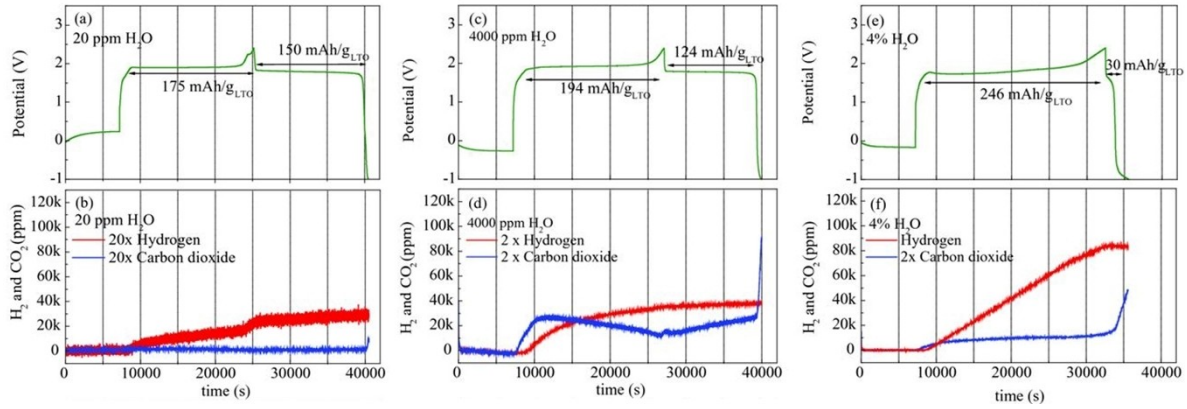

Figure 5. Cell potential versus time during the galvanostatic charge and discharge of an LTO//LFP full-cell at C/5 (0.39 mA) using 80 μL 1 M LiTFSI in EC/EMC (3/7 g/g) in a 1-compartment cell configuration (s. Figure 1a): a) without intentionally added water, c) with 4000 ppm H_2O, and e) with 4% H_2O. Note that the theoretical discharge capacity for the capacity limiting LTO electrode corresponds to 18000 s (C/5). Figures b), d), and f) show the corresponding real-time H_2 and CO_2 concentration in the cell determined by the OEMS (for better legibility, some of the gas concentration signals were multiplied by a magnification factor indicated in the figure). All measurements start with an initial 2 h OCV period of the as-assembled cell (i.e., in its discharged state). Reprinted with permission2014 IOP Ltd.[39]

the positive electrode material.[53] Regardless, it is widely agreed that water can lead to substantial H_2 generation that could increase risk during cell manufacturing and operation.

The water reduction occurs at the negative electrode surface (i.e., low potentials), which is responsible for the H_2 evolution:[47b]

$$H_2O + e^- \rightarrow OH^- + {}^1/_2H_2\ (g) \quad (3)$$

Experimentally, many studies have observed the H_2 gas evolution in LIB cells.[30,39–40,47,54] Wu et al. investigated the influence of the moisture in electrolytes on the pouch cell swelling and found that the formed gas volume is monotonically correlated with the water content from 0 ppm to 20,000 ppm.[54b] This is consistent with the idea that the H_2 is generated via the electrochemical reduction of water. Moreover, Bernhard et al. intentionally introduce moisture into the LTO//LFP cells before undergoing cycling. The results presented in Figure 5 showed that 20 ppm, 4,000 ppm, and 40,000 ppm water contents gave 0.51 μmol, 7.4 μmol, and 31 μmol of H_2, respectively.[39] Similar behaviors were also observed in the cell with a graphite anode. Table 1 shows that only 250 ppm (ca. 0.1 μmol) H_2 was detected in the cell with 20 ppm moisture content, which shoots up to 8,000 ppm (ca. 2.1 μmol) H_2 when the moisture content is increased to 4,000 ppm.[40] It is reported that the quality of the SEI grown on graphite anodes could be severely destructed at elevated temperatures to produce gases, resulting in a shorter cycle life and a higher cell resistance.[47a,55] Substantial amounts of H_2 gas, together with CO_2 may be formed during this process if the electrolyte is contaminated by moisture.[56] A vinylene carbonate (VC) containing SEI on graphite was found to be effective in suppressing the formation of H_2 gas.[40] Table 1 confirms that a significantly smaller amount of H_2 gas was detected in the cell with the same moisture content if a proper SEI was formed using the VC-containing electrolyte blends.

Table 1. Overview of evolved amounts of hydrogen (H_2) in units of [ppm] and [μmol H_2], as quantified by OEMS for wet and dry electrolytes with pristine and SEI-protected graphite anodes. The OEMS measurements were performed in 1 M LiTFSI in EC/EMC; with either < 20 ppm H_2O (< 0.16 μmol H_2O) or 4000 ppm H_2O (32 μmol H_2O). Assuming a one-electron reduction reaction of water to OH^- and H^+, the former could result in a maximum H_2 release of 0.08 μmol H_2, and the latter could result in 16 μmol H_2 (compared to the experimentally determined concentrations in the Table). The data are collected with permission 2015 CC BY NC ND 4.0.[40]

Electrode condition/H_2O content	Accumulated amount of H_2 gas in experiments			
	After 1st cycle		After 3rd cycle	
Fresh graphite/ 20 ppm	250 ppm	0.1 μmol	250 ppm	0.1 μmol
Fresh graphite/ 4,000 ppm	8,000 ppm	2.1 μmol	12,000 ppm	4.7 μmol
After formation/ 4,000 ppm + 2% VC	600 ppm	0.2 μmol	1,600 ppm	0.6 μmol

In industrial production, the moisture-induced H_2 formation is largely mitigated by a degassing step (by venting for cylindrical cells or by resealing for pouch cells) after the formation cycle. The potential for most anodes is sufficiently low to facilitate a complete water reduction, which peaked at ca. 1.2 V vs. Li/Li^+.[57] For instance, common LIB anodes often have redox potentials below ca. 0.5 V vs. Li/Li^+, regardless of whether they are the commercial ones, such as graphite and graphite-Si blends, or the lab scale ones, such as Si-, Ge-, Sn-, and Al-alloy.[58] Bernhard et al. reported that the onset potential for water reduction is ~1.6 V vs. Li/Li^+ for the graphite anode during the initial cycle, but could decrease to ~0.8 vs. Li/Li^+ in the 2nd and 3rd cycles owing to the protection of a proper SEI layer.[40]

The H_2 gassing issue could become more pronounced in the cells with LTO anodes in the absence of a protective SEI layer due to its high redox potential, i.e., ~1.55 V vs. Li/Li^+.[59] Therefore, the LTO anode should be discussed separately from other anode candidates. Although the onset potential for water reduction can be as high as ~2 V vs. Li/Li^+,[60] the moisture largely remains in the LTO electrode even after the formation cycles, thereby inducing H_2 formation via:[39]

$$Li_7Ti_5O_{12} + 3H_2O \rightarrow Li_4Ti_5O_{12} + 1.5H_2\ (g) + 3Li^+ + 3OH^- \quad (4)$$

Furthermore, the presence of moisture may catalyze the formation of other gaseous species via the decomposition of the PF_6^- containing electrolytes. Wu et al. quantitatively analyzed the gaseous products in the NMC//LTO pouch cell after cycling or storage at the charged state in the temperature range between 40 °C and 80 °C. H_2 gas was found to account for more than 70% of the total gas volume when a typical LP30 electrolyte is in use.[54b] While a consensus is reached that residue moisture should be largely responsible for the H_2 gas formation, He et al. utilized OEMS and concluded that H_2 gas is still one of the primary gas products in the LTO electrode in the initial charge when the water content in the EC-containing electrolyte is limited to $\leq$15 ppm.[61] This conclusion can be further supported by some other studies, in which various cell chemistries were used and the water content was strictly controlled. H_2 gas was detected as a major gaseous species in the NMC 532//Graphite cell with LP57 electrolyte ($\leq$2 ppm H_2O),[22] the NMC 622//Graphite cell with LP57 ($\leq$20 ppm H_2O; the electrodes were dried at 80 °C for 14 hours),[30] NMC 111//Graphite cell ($\leq$20 ppm H_2O; the electrodes were dried at 95 °C for 12 hours),[42] the LTO//Li half cell with LP47 ($\leq$20 ppm or $\leq$10 ppm H_2O; the electrodes were dried at 100 °C for 10 hours),[39,62] and the LTO//LMO cell with various electrolytes.[47b]

Apart from the water reduction, several pathways are proposed to be responsible for H_2 gas evolution in LIBs. It is emphasized that the present report sets out to summarize published mechanisms, although some of them may be disputed. For example, the LTO surface may be catalytic to the dehydrogenation of the alkoxy groups in the electrolyte solvents,[54a] leading to H_2 gas evolution, as reported in Equation 5. That said, such a biradical seems unlikely to ever exist. It is perhaps more likely that such a reaction occurs via proton transfer steps and a two-electron Faradaic reduction step. Regardless, the reduction of organic carbonate solvents is completely expected, even if the pathway to H_2 gas is not universally recognized.

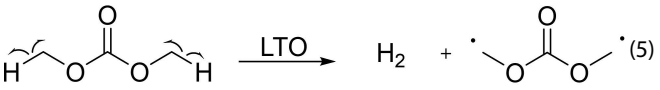

(5)

Moreover, the reaction of Li with LiOH reported by Schechter et al. (Equation 6),[63] and the electrocatalytic transformation of HF impurity into H_2 and LiF (Equation 7),[64] are also the proposed routes for H_2 gas formation. It is here emphasized that both may be understood as the reduction of protic species, e.g., acids and alcohols:

$$LiOH + Li^+ + e^- \rightarrow Li_2O + {}^1/_2H_2\ (g) \quad (6)$$

$$HF + Li^+ + e^- \rightarrow LiF + {}^1/_2H_2\ (g) \quad (7)$$

It should be further noted that HF is one of the decomposition products of the electrolyte salt $LiPF_6$ in the presence of moisture or at elevated temperatures.[65] Moreover, it is suggested that the reduction of protic species derived from electrolyte oxidation (at the cathode side) or introduced by slurry additives might also be another source of H_2, in addition to the water reduction:[42,66]

$$R{-}H^+ + e^- \rightarrow R + {}^1/_2H_2\ (g) \quad (8)$$

$$ROH + e^- \rightarrow RO^- + {}^1/_2H_2\ (g) \quad (9)$$

To summarize, the residual moisture in LIBs is considered one of the primary sources for the H_2 evolution.[39,56] The mechanism of H_2 evolution occurring in cells with minimized moisture content remains disputed and unclear.[61] For instance, Michalak et al. observed a potential-dependent evolution of H_2 when charging a graphite//Li cell to 1.2 V, and suggested that the H_2 gas originates from the SEI destruction.[67] Galushkin et al. concluded that H_2 gas may be a consequence of the electrochemical reaction of electrolyte and/or SEI decomposition, even if the moisture content is limited. Therefore, other pathways that may induce H_2 gas generation in LIBs should not be neglected. Possible reactions include the decomposition of EC and its subsequent reduction of water by CO but requiring further investigations:[68]

$$C_3H_4O_3(EC) \rightarrow 2H_2(g) + 3CO \quad (10)$$

$$CO + H_2O \rightarrow H_2(g) + CO_2 \quad (11)$$

3.2. C_2H_4 Evolution in Li-ion Batteries

C_2H_4 is a common gas that is usually observed in various LIB cells with EC-containing electrolyte blends, including NMC//Graphite, NMC//LTO,[54b] LMO//LTO,[47a] and LTO//Li.[61–62] Ellis et al. utilized the AISGA technique and quantified that C_2H_4 is the second abundant gas after the initial charge process of an NMC//Graphite cell.[30] As shown in Figure 6a, two evident gassing events are highlighted by the arrows, namely below ~3.5 V and above ~4.2 V. Then Figure 6b makes it clear that most C_2H_4 gas was generated during the first gassing event (grey portion), together with the quantitative data of other gases. C_2H_4 evolution is reported to originate from the break-

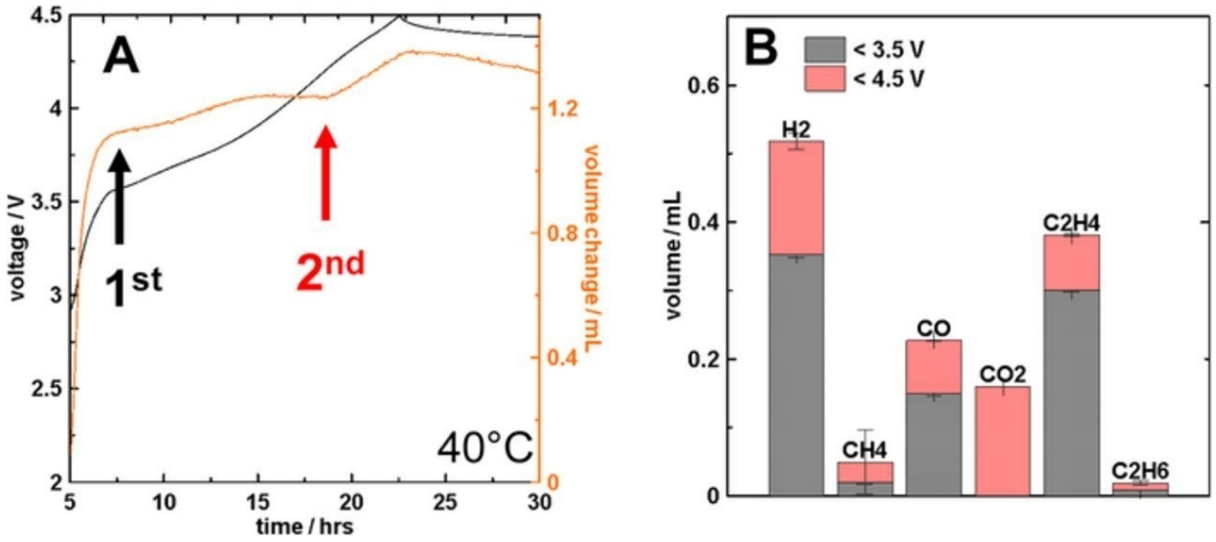

Figure 6. a) Voltage vs time and volume change vs time for a fresh lithium-ion cell during the first charge cycle. b) the composition of the gas, measured by GC-TCD (gas chromatography-thermal conductivity detector), evolved from the cell in (a) during the first charge. Reprinted with permission 2017 CC BY 4.0.[30]

down of electrolyte solvents, more specifically, from the SEI formation (e.g., reduction of EC to form lithium ethylene dicarbonate, LEDC)[60–61,69] and/or possible SEI decomposition[67,69d] via:

$$(CH_2O)_2CO + Li^+ + e^- \rightarrow {}^1/_2C_4H_4Li_2O_6 + {}^1/_2C_2H_4\ (g) \quad (12)$$

$$(CH_2O)_2CO + 2Li^+ + 2e^- \rightarrow Li_2CO_3 + C_2H_4\ (g) \quad (13)$$

$$(CH_2OCO_2Li)_2 \rightarrow Li_2CO_3 + C_2H_4\ (g) + CO_2 + \frac{1}{2}\ O_2 \quad (14)$$

$$(CH_2OCO_2Li)_2 + 2Li \rightarrow 2Li_2CO_3 + C_2H_4\ (g) \quad (15)$$

Furthermore, Metzger et al. conducted an OEMS study using Graphite//Li half cells that underwent CV scans. They observed C_2H_4 formation when the potential is lower than ~0.8 V vs. Li/Li^+.[42] As illustrated in Figure 7, the C_2H_4 concentration starts shooting up as soon as the negative CV sweep approaches ~0.8 V vs. Li/Li^+ (red vertical line) until the end of the first discharge (i.e., 0 V). The constant signal of C_2H_4 afterward indicates that the reduction of EC likely stopped as soon as a sufficiently stable SEI was formed.[42] This agrees with the observation that C_2H_4 evolution was only pronounced during the initial charging when SEI was being deposited.[40] Many studies suggest that the reduction of EC is the main origin of C_2H_4 gas via Equation 10.[30,40,42,61–62,69b,70] The conclusion is well supported by an electrolyte comparison study, where a significantly higher C_2H_4 content was found in the NMC//LTO cell with the LP30 (i.e., EC + DMC). Whereas all the other electrolyte blends, including DMC, DEC, PC + DMC, and PC + DEC, did not exhibit substantial C_2H_4 gas evolution.[54b]

3.3. CO Evolution in Li-ion Batteries

As can already be seen in Figure 6 and Figure 7, CO is one of the common gaseous species in LIBs during operation and should draw extra attention due to its toxicity.[71] The situation of CO evolution can be rather complicated as it may be formed via either reduction or oxidation, e.g., reduction of EC or oxidation of carbonaceous species inside LIB cells.[41]

While the reduction of EC is believed to be responsible for C_2H_4 evolution via the formation of LEDC, as discussed in the previous section (Scheme 1A), Onuki et al. used isotope-labeled electrolyte solvents and concluded that the main source for CO is also via the reduction of EC (Scheme 1B), where the position of the ring opening is different.[69b] It is suggested that EC can coordinate with PF_6^- anions, forming radical EC^{*+} cations at the cathode of the LIB. Xing et al. proposed five possible pathways based on theoretical calculations to illustrate the decomposition of the EC^{*+}, which is suggested to be responsible for the formation of CO and CO_2.[72]

Also, Strehle et al. realized the mismatch between capacity contributed by the EC reduction ($2e^-$ per C_2H_4 molecule) and the total charge harvested from the reduction current. The authors suggested that other reduction reactions must occur in addition to those leading to C_2H_4 formation.[70] Many studies have observed the formation of CO during the reduction in several electrolyte blends, such as EC/DMC[73] and EC/EMC,[69b,74] of which the co-solvents were reported to be also responsible via:

$$DMC + 2Li^+ + 2e^- \rightarrow CH_3OLi + CO\ (g) \quad (16)$$

$$EMC + 2Li^+ + 2e^- \rightarrow CH_3OLi + EtOLi + CO\ (g) \quad (17)$$

Although no solid evidence can be found on whether EMC could be reduced to form CO, the trans-esterification between EMC and DMC + DEC is suggested by Yoshida et al.[74] Trans-

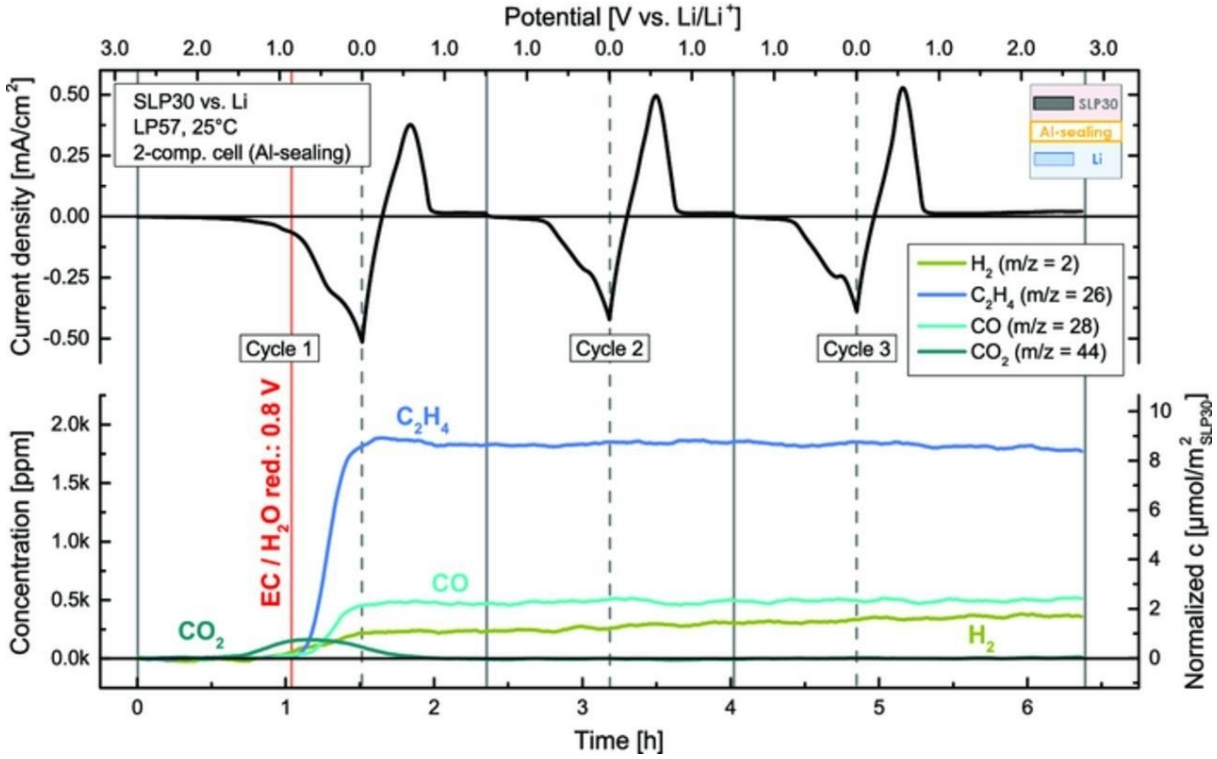

Figure 7. Gas evolution during the first three formation cycles of an SLP30 (Gr)//Li half-cell at 25 °C in an Al-sealed two-compartment cell with 80 µL LP57 in the working-electrode compartment connected to the OEMS. Upper panel: current-potential curve for CV formation procedure between 0–1.5 V vs. Li/Li^+ at $\nu = 0.5$ mV/s. Lower panel: gas concentration in the cell head space during formation in units of [ppm] and [µmol/m² SLP30] for H_2 (m/z = 2), C_2H_4 (m/z = 26), CO (m/z = 28), and CO_2 (m/z = 44) (4 h OCV phase not shown). Reprinted with permission 2016 CC BY NC ND 4.0.[42]

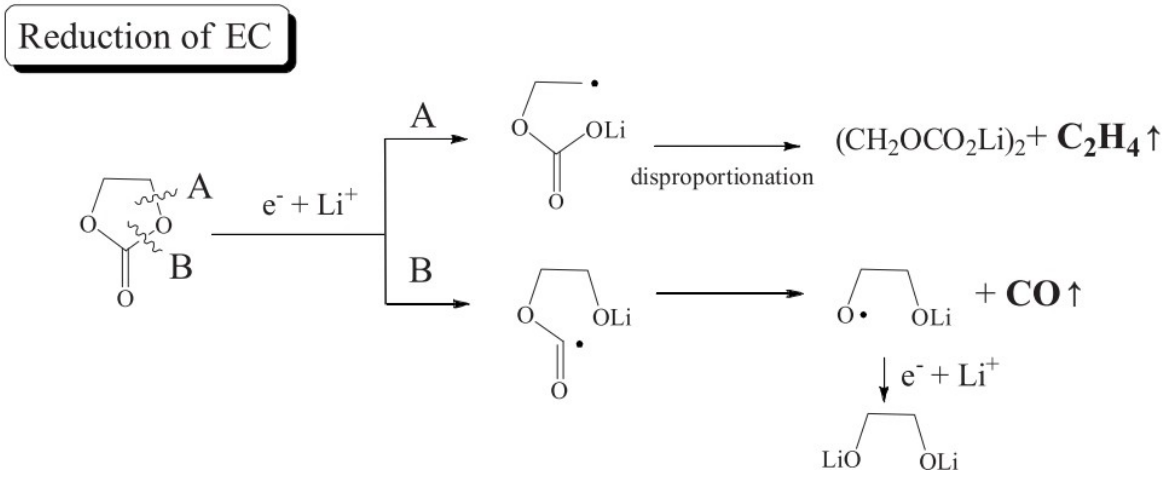

Scheme 1. Proposed mechanism of Onuki et al. for the generation of CO via the reduction of EC. It is noted this is considered a minor reaction product, where the major products are LEDC and C_2H_4. Reprinted with permission 2008 IOP Ltd.[69b]

esterification is well-documented to occur by post-mortem analysis by GC-MS and is widely agreed to occur via reactions of nucleophilic alkoxides (i.e., LiOMe, LiOEt) with the carbonyl carbon of the organic carbonates. In any case, EMC may still be considered one of the sources for the CO formation following Equation 17. The discussions so far agree nicely with the experimental observation that CO evolves simultaneously with C_2H_4, as both gases are generated via reduction reactions that could possibly be occurring simultaneously.[42]

Apart from the reduction, oxidations (at the cathode) of non-electrolyte components inside are also reported to contribute to the CO formation. For example, Onuki et al. realized that only about two-thirds of the formed CO and CO_2 originate from the electrolyte.[69b] The authors speculated that the conductive carbon and/or the PVdF binder should be responsible. Later,

Metzger et al. conducted a systematic study to clarify the gas contributions by distinguishing the weight loss from (a) the conductive carbon and (b) the electrolyte from the oxidation reactions.[41] It is suggested by the authors that the CO and CO_2 evolution should be partly responsible for the observed weight loss in conductive carbon via:

$$C + H_2O \rightarrow CO\ (g) + 2H^+ + 2e^- \quad (18)$$

$$C + 2H_2O \rightarrow CO_2 + 4H^+ + 4e^- \quad (19)$$

As can be seen from Figure 8, the weight losses in both conductive carbon and electrolytes were found to be strongly correlated to the water content as well as the operation temperature. It should be noted that the voltage window used in the study was extraordinarily high (e.g., up to 5.5 V), the CO/CO_2 evolution is recorded at voltages beyond 4.5 V, but it will become a different story under elevated temperatures or there is water contamination.[41] Since the anodic oxidation reactions generate both CO and CO_2, they will be discussed together in the next section.

Regarding electrode materials, LTO and NMC electrodes should be discussed independently. The dehydrogenation reaction of alkoxy carbonates may be catalyzed by the LTO surface to form H_2. The subsequent decarboxylation reactions of the formed intermediates are reported to promote CO formation via:[75]

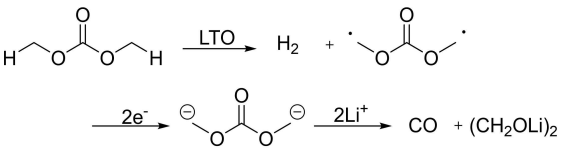

(20)

In the case of NMC, the O_2 release from its lattice may lead to the oxidation of EC, forming CO, CO_2, and H_2O via:[43a]

$$(CH_2O)_2CO + O_2 \rightarrow CO\ (g) + 2CO_2 + 2H_2O \quad (21)$$

Lastly, regardless of the cell components, CO gas may be produced by the reduction of CO_2 by Li^+ (Equation 22).

$$2CO_2 + 2Li^+ + 2e^- \rightarrow CO\ (g) + Li_2CO_3 \quad (22)$$

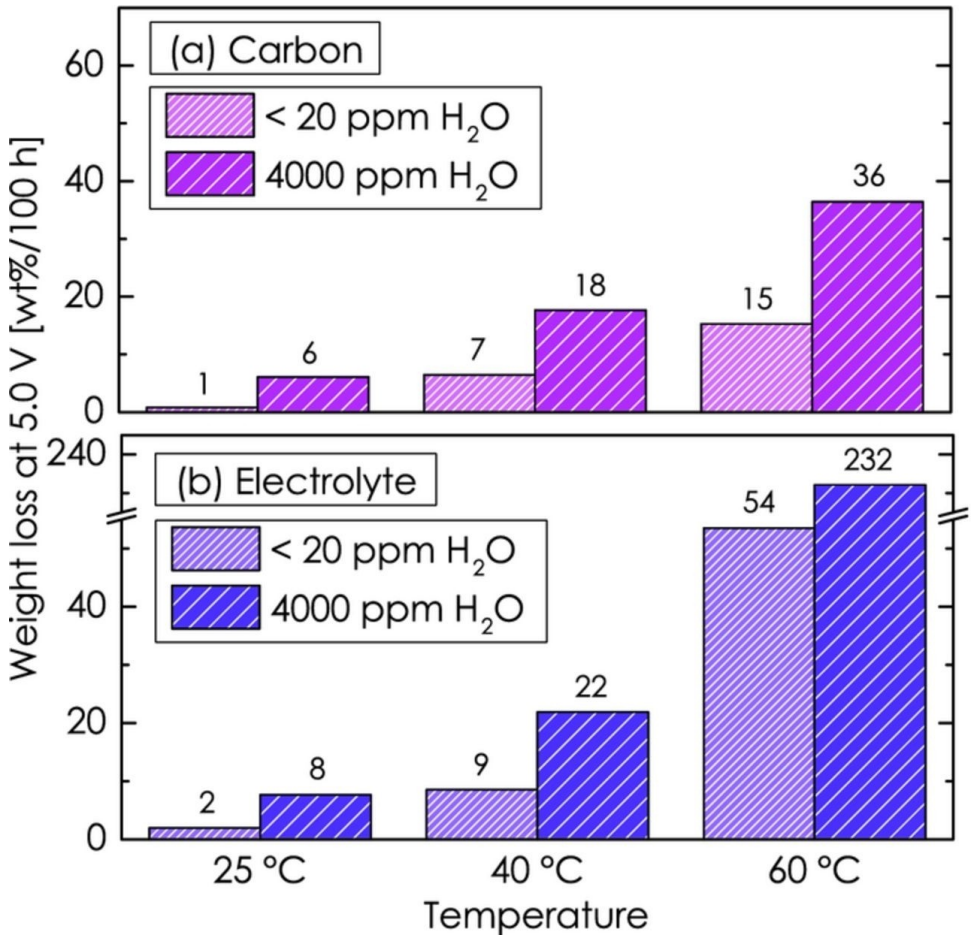

Figure 8. Accumulated weight loss of conductive carbon (a) and electrolyte (b) over 100 h at a potential of 5.0 V for temperatures of 25, 40, and 60 C with $<$ 20 ppm H_2O and with 4000 ppm H_2O. Reprinted with permission 2015 BY NC ND 4.0.[41]

3.4. CO_2 Evolution in Li-ion Batteries

The breakdown (oxidation) reactions of electrolytes leading to CO_2 formation are provided,[76] in addition to the reaction in Scheme 1B before:

$$RCO_3R \rightarrow ROR + CO_2\ (g) \tag{23}$$

$$(CH_2O)_2CO + H_2O \rightarrow (CH_2OH)_2 + CO_2\ (g) \tag{24}$$

Equation 23 generalizes the oxidation of organic carbonates occurring at the cathode surface when the potential is sufficiently high.[27,77] Meanwhile, the self-driven hydrolysis reaction from EC to ethylene glycol is reported to occur in the presence of Lewis bases, thus producing CO_2. This process, however, is independent of the cell voltage (Equation 24).[78] According to the water reduction presented in Equation 3 (pronounced during the initial charge), the hydroxide ion (OH^-) is a stronger nucleophile than H_2O, resulting in a faster reaction rate than the hydrolysis of EC.[41] Also, it is crucial to revisit Equation 21 that EC can be oxidized in the presence of O_2 to generate CO_2 and H_2O, of which the latter may facilitate secondary CO_2 formation via Equation 24.

Together with the conductive carbon oxidation, as presented in Figure 9a, it is reported that CO is absent at room temperature (25 °C) when the electrolyte is sufficiently dry ($\leq$ 20 ppm H_2O) while the oxidation reactions only generated CO_2 at potentials higher than ca. 4.8 V.[41] With the ^{12}C-carbon black and the $^{13}C_3$-EC (isotope-labeled), one can distinguish the CO_2 contributions of the oxidation of the former (Equation 19) and the latter (Equation 23). Either increasing the water content to 4,000 ppm (Figure 9b) at the same temperature or increasing the temperature to 60 °C (Figure 9c) with the same water content would lead to the formation of CO and a more pronounced formation of CO_2. In both cases, the onset potentials for the corrosion current and the CO/CO_2 evolution are shifted negatively. Interestingly, the higher temperature seems to play a more important role in facilitating the CO_2 evolution, giving ca. 3,000 ppm at 60 °C with 20 ppm H_2O vs. ca. 600 ppm at 25 °C with 4,000 ppm H_2O. The role of temperature can be well supported by Sloop et al., who observed the CO_2 evolution by simply heating the electrolyte.[79] When both moisture and temperature are increased (i.e., 4,000 ppm H_2O and 60 °C), the CO_2 evolution from the oxidation of EC alone can reach a level as high as ca. 13,000 ppm (Figure 9d). It should be noted that the oxidation of conductive carbon was also greatly enhanced by the higher moisture and temperature, although not as evident as that of EC.

Other reactions that drive the CO_2 formation were also reported, in addition to the oxidation of electrolyte and/or conductive carbon.[80] As discussed, CO_2 can be expected when cells are cycled to higher voltages due to the oxidation of electrolytes (Equation 21).[81] In the presence of large amounts of CO_2, the lithium carbonate (Li_2CO_3) formation described in Equation 22 is likely facilitated, which may further react with the electrolyte salt (e.g., $LiPF_6$) to release secondary CO_2 via:[82]

$$LiPF_6 + Li_2CO_3 \rightarrow CO_2(g) + 3LiF + POF_3(g) \tag{25}$$

$$LiPF_6 + 2Li_2CO_3 \rightarrow 2CO_2(g) + 4LiF + F_2PO_2Li \tag{26}$$

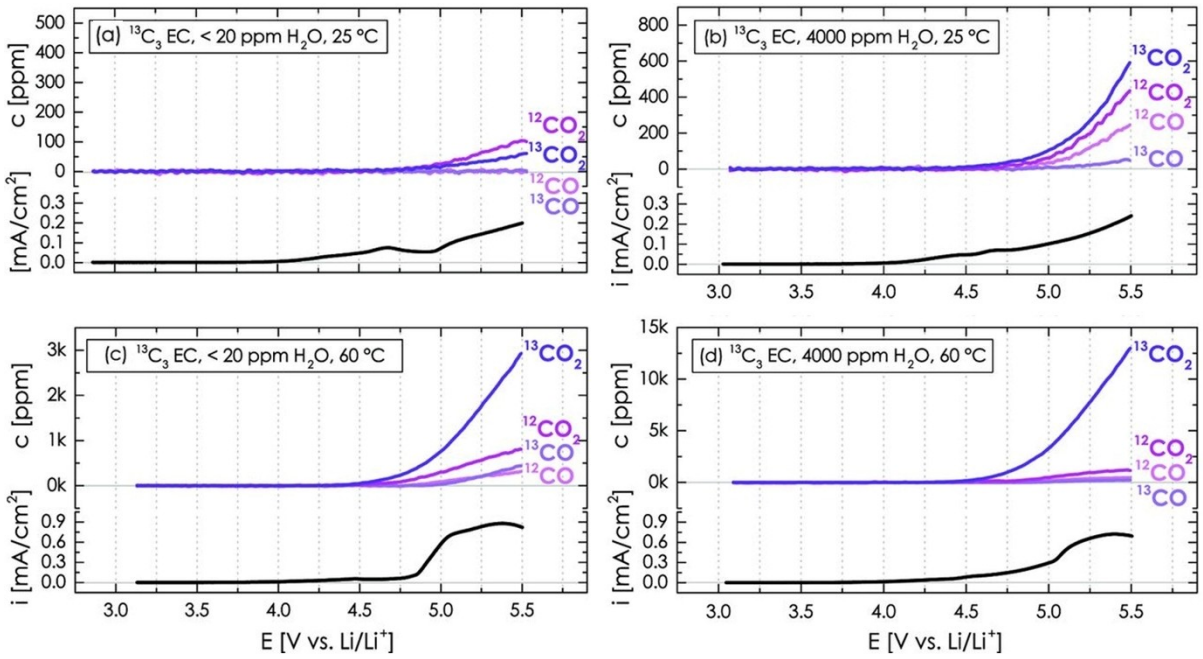

Figure 9. Temperature and water effect on the CO_2 and CO evolution as well as on the overall oxidation current during the anodic oxidation of a Super C65/PVdF (50/50 wt/wt) working-electrode with 4000 ppm H_2O-containing 2 M $LiClO_4$ in isotopically labeled $^{13}C_3$ EC (240 µl) during a LSV scan from OCV to 5.5 V vs. Li/Li^+ at 0.2 mV/s. The lower-compartment with a lithium metal counter-electrode contains 160 µl dry non-labeled $^{12}C_3$ EC with 2 M $LiClO_4$. Adapted with permission 2015 BY NC ND 4.0.[41]

Li_2CO_3 together with other SEI components, such as lithium methyl carbonate (LMC) and LEDC, may thermally decompose in the presence of $LiPF_6$ salt and DMC solvent via:[82]

$$LiPF_6 + 3LMC \rightarrow 3CO_2(g) + 4LiF + OPF_2OCH_3 + CH_3OCH_3 \quad (27)$$

$$OPF_2OCH_3 + LMC \rightarrow LiF + CO_2 + OPF(OCH_3)_2 \quad (28)$$

$$LMC(LiPF_6\ as\ the\ catalyst) \rightarrow CO_2 + CH_3OLi \quad (29)$$

$$(CH_2CO_2Li)_2\ (LEDC) + trace\ H_2O \rightarrow CO_2 + Li_2CO_3 + (CH_2OH)_2 \quad (30)$$

These reactions refer to some of the well-known organic chemical processes, namely transesterification, etherification, and decarboxylation.[83] All the products described in the equations above are observed from the decomposition of LEDC when the electrolyte of $LiPF_6$ in DMC is being used.[75,82] Last but not least, it should be noted that HF may form if moisture is introduced to the cell either during battery production or operation. In this case, lithium alkyl carbonate (LAC) will decompose in the presence of HF, leading to the formation of CO_2:[46b,69e]

$$LiOCO_2CH_3 + HF \rightarrow LiF + CH_3OH + CO_2 \quad (31)$$

Concerning the electrode materials, Ti^{4+} in LTO can coordinate with the oxygen of the carbonyl group of linear carbonates and initiate reactions to produce CO_2 and other by-products. Also, the Ti^{4+} can catalyze the ring-opening polymerization of cyclic carbonates (e.g., EC) to form CO_2 and PEO-like oligomers $(–CH_2–CH_2–O–)_n$ as follows:[54a,75]

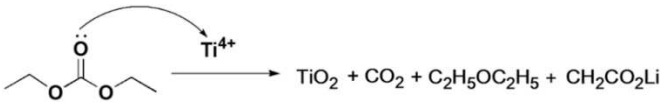

(32)

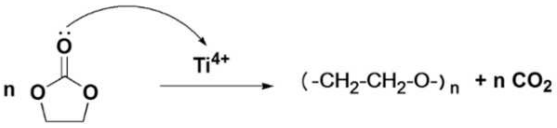

(33)

The ring-opening polymerization can also be triggered by PF_5, which is the product of the decomposition of $LiPF_6$ salt in electrolytes. As a strong Lewis acid, PF_5 can cleave the ether linage of cyclic and/or linear carbonate to liberate CO_2:[84]

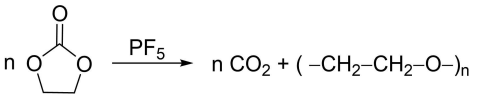

(34)

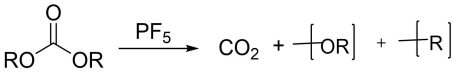

(35)

3.5. O_2 Evolution in Lithium-Ion Batteries

Different from the gases that are previously discussed, O_2 gas is believed to mainly originate from lattice oxygen release in the high-voltage cathodes.[43a,85] Taking the nickel-rich layered lithiated NMC cathodes as examples, Streich et al. found that the Ni content is the key factor in governing the onset and rate of O_2 evolution (Figure 10) when the cell voltage goes beyond 4.3 V. Rinkel et al. found the onset of gas evolution and O_2 release is better linked with the electrode state of charge, occurring at 80–84% for LCO and for several NMC compositions (33–80% Ni).[46b] This correlation suggests that the surface reconstruction of NMCs and accompanied electrolyte decomposition should be responsible for the O_2 gas release. Ni–O_2* surface states (and their interactions with Co) are reported to alter the structural stability of NMC electrodes.[86]

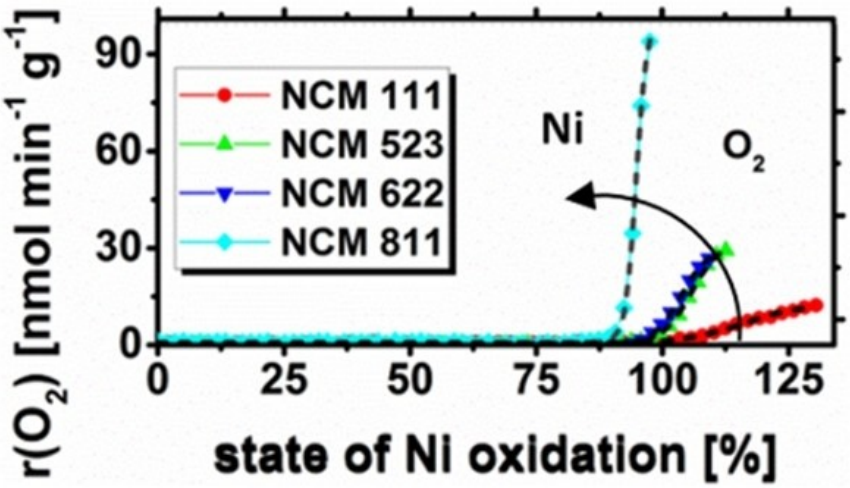

Figure 10. Dependence of O_2 evolution on the state of Ni oxidation during 1st charge. Reprinted with permission 2017 American Chemical Society.[86]

Furthermore, it is experimentally observed that Li-rich cathodes in general release much more O_2, in comparison with Li-stoichiometric NMCs, owing to intensified anionic redox reactions, hence the over-oxidation of the peroxo-like species.[85b,87] For example, Tarascon's group has reported a wide range of layered cathode materials, such as $Li_{1.2}Ni_{0.13}Mn_{0.54}Co_{0.13}O_2$,[87c] $Li_{1.17}Ti_{0.33}Fe_{0.5}O_2$,[87b] $Li_{1.17}Ti_{0.58}Ni_{0.25}O_2$,[88] $Li_{1.09}Ni_{0.85}Mo_{0.06}O_2$,[87a] and $Li_{1.2}Ni_{0.2}Mn_{0.6}O_2/Li_{1.2}Co_{0.4}Mn_{0.4}O_2$,[89] all of which release oxygen at high potentials. A structural densification event is observed after the first charge, and an almost negligible amount of oxygen release is observed from the second cycle onward. It is also worth noting that, in addition to oxygen released from the lattice, Mahne et al. proposed that electrochemical oxidation of surface Li_2CO_3 impurities may generate highly reactive singlet oxygen ($^1O_2$) above 3.8 V vs. Li/Li^+, which will subsequently react with carbonate electrolytes and release CO_2.[90]

3.6. Gas Consumption in Lithium-Ion Batteries

While the gas sensing technologies capture the gas evolution nicely, gas consumption may be overlooked when the evolved gases are being sampled continuously like the DEMS. Therefore, this sub-section focuses on discussing the possible gas consumption pathways.

Consumption of H_2. H_2 is found to be consumed by both the NMC cathode and the graphite anode, of which a more pronounced consumption is observed by the latter at the same SoC. Ellis et al. demonstrated the H_2 consumption by the lithiated graphite anode and proposed the possible reduction of H_2 by Li:[30]

$$2Li + H_2 \rightarrow 2LiH \tag{36}$$

Strong temperature dependence was observed in this reaction with ca. 6 times more H_2 consumed at 60 °C than that at 40 °C, suggesting that the reaction shown in Equation 36 may not be kinetically favorable at lower temperatures.[30] The produced LiH can be reactive to other components, such as electrolyte solvents in a full cell to form OH^-. The OH^- species could facilitate the dissolution of the transition metals from the cathode and catalyze EC decomposition, affecting the cycling life of the cell.[30]

Consumption of C_2H_4. C_2H_4 can also be consumed at the graphite anode in its charged state with a strong temperature dependence. ~0.2 mL and ~1.6 mL of C_2H_4 were found to be consumed after storing the cell at 40 °C and 60 °C, respectively. A series of reactions are proposed:[91]

$$2Li + C_2H_4 \rightarrow Li_2C_2H_4 \tag{37}$$

$$Li_2C_2H_4 + C_2H_4 \rightarrow 2LiC_2H_4 \tag{38}$$

$$LiC_2H_4 + nC_2H_4 \rightarrow Li(C_2H_4)_{n+1} \tag{39}$$

Through the reactions described in Equation 37–39, ionic polymerization of C_2H_4 makes it possible to form polyethylene, resulting in the thickening of SEI on the anode surface.[92] C_2H_4 is also found to be reactive to the NMC cathode, giving a higher charge transfer impedance but with no evident consumption of C_2H_4.[30] Either a cathode-electrolyte interphase (CEI) or a rock salt layer (RSL) forming on the surface of the cathode can be significantly thinner than an SEI layer on the anode, resulting in this minor C_2H_4 consumption at the cathode. In any case, Ellis et al. suggest that the reaction between C_2H_4 and the cathode might be irrelevant in a full cell, as the consumption of C_2H_4 at the anode competes with that at the cathode.[30]

Consumption of CO. The consumption of CO is trivial and does not seem to exhibit temperature dependence. A small amount of CO is consumed after storage for 100 hours. No continuous consumption is observed afterward, indicating that only a part of CO is consumed during storage, i.e., residue CO may be expected in the cell after long-term storage or usage.[30] According to Equation 11, CO might be consumed by residue moisture to form H_2 and CO_2, representing one of the cross-talks among gases inside battery cells.

Consumption of CO_2. CO_2 was used as an additive and is consumed to form Li-rich SEI on anodes in the early days,[93] but the subsequent effects on cell health remain unclear. CO_2 has the highest redox potential compared to other species in the electrolyte, and it is reported to be likely consumed at lithiated anodes to form $Li_2C_2O_4$ via:[79]

$$2Li + 2CO_2 \rightarrow Li_2C_2O_4 \tag{40}$$

Later, one study nicely supports the reaction in Equation 40, which proves the existence of an oxalate-type compound or semi-carbonate on the surface of the graphite anode.[30] This CO_2 reduction reaction is reported to occur at potentials below 2.8 V vs. Li/Li^+.[79] Considering the low potential of graphite anodes, CO_2 should be continuously consumed in the battery cells during operation and storage as long as Li is present in the anode. This argument agrees with the observation from Ellis et al. that CO_2 is found to be completely consumed while H_2, C_2H_4, and CO are partly consumed after storage.[30]

3.7. Other Gaseous Species in Lithium-Ion Batteries

Apart from the five major gases discussed above, other gaseous species may also be present in LIBs during their formation, cycling, and storage. Hydrocarbons like CH_4 and C_2H_6,[30,47b,56] and C_2H_2,[76e] are observed in Li-ion cells from time to time but are minorities. PF_5 gas, which is often observed as POF_3 gas owing to its reactivity with trace water and other reactive species in the cell, signifies the degradation of the electrolyte salt $LiPF_6$ and can be readily quantified by OEMS.[65,94] Understanding the origin, evolution, and fate of these minor gases may also be crucial. It should be noted that gassing events can vary a lot in cells with different chemistries. In some drastic cell failures like thermal runaway, safety venting may lead to the release of particular matters as evidenced by mass loss.[12] While

these gaseous species are beyond the scope of this review, their safety concerns should not be neglected in future discussions. Given that this chapter discusses lots of gassing pathways, Table 2 which summarizes the possible origins and reaction pathways of H_2, C_2H_4, CO, CO_2, and O_2 is provided for easy reference.

4. Limitations of the Gas Sensing Technologies

Despite the BMS being integrated into modern EVs, incidents like swelling, thermal runaways, etc. may still take place. Solely measuring temperature and strain may not be enough to prevent incidents or offer early warnings. This section discusses why the currently available gas sensing techniques cannot be easily integrated with commercial battery products, by highlighting their limitations.

4.1. Gas Species in VSGA

As an experimental apparatus developed in the 1980s, VSGA exhibited high precision in determining the gas volume evolved in battery cells. However, the qualitative analysis is absent, such that the gas nature remains a mystery. Also, since the cell was primarily designed to conduct lab-scale experiments, it can hardly be applied to commercial batteries.

4.2. Cell Type in AISGA

The AISGA technique could monitor the change in the gas quantity of pouch cells in operando with great accuracy, but only pouch cells exhibit evident package expansion or swelling which validates Archimede's principle. Other battery formats with rigid casing, such as cylindrical or prismatic cells, cannot be measured using the technique. While AISGA is considered an in situ technique, the determination of gas nature is in fact ex situ since only a handful of sampling attempts are made during one charge-discharge cycle. For example, Ellis et al. took sample

Table 2. Summary of possible sources, and triggering conditions of the five main gases observed in LIBs with different cell chemistries.

Gas	Possible source	Triggering condition	Potential (vs. Li/Li^+)	Cell chemistry	Ref.
H_2	H_2O and H^+ species	Reduction at anode	$\leq$1.6 V	Graphite//Li, LiTFSI in EC/EMC	[40]
	EC decomposition	Reduction at anode	n/a	NMC//Graphite, $LiPF_6$ in EC	[68]
	SEI destruction	High anode potential	$\geq$~0.9 V	Graphite//Li, $LiPF_6$ in EC/EMC	[67]
C_2H_4	EC decomposition	Reduction at anode	$\leq$0.8 V	NMC//Graphite, $LiPF_6$ in EC/EMC	[42]
	SEI destruction*	High anode potential	$\geq$~0.9 V	LNMO//Graphite, $LiPF_6$ in EC/EMC	[67]
CO	Conductive carbon	High cathode potential	$\geq$~5 V	Super C65 + PVdF//Li, $LiClO_4$ in EC	[41]
	EC decomposition	Reduction at anode	n/a	NCA//Graphite, $LiPF_6$ in EC/DEC	[69b]
	DMC decomposition	Trans-esterification	n/a	LCO//Graphite, $LiPF_6$ in DMC	[74]
CO_2	Conducive carbon	High cathode potential	$\geq$~5 V	Super C65 + PVdF//Li, $LiClO_4$ in EC	[41]
	Electrolyte oxidation	Oxidation at cathode	$\geq$~4.4 V	LCO//Li, $LiPF_6$ in EC/DEC	[76b]
	EC hydrolysis	Temperature ($\geq$40 °C)	n/a	$LiClO_4$ in EC with 4,000 ppm H_2O	[41]
	SEI decomposition	Temperature ($\geq$55 °C)	n/a	Li_2CO_3, LMC, LEDC//$LiPF_6$ in DMC	[82]
	LAC decomposition	Presence of HF	n/a	LNMO//Graphite, $LiPF_6$ in EC/EMC	[69e]
	Carbonates decomposition	Presence of PF5	n/a	$LiPF_6$ in EC, DEC, EMC, DMC	[84]
	Li_2CO_3 oxidation	Intermediate cell voltage	>~3.8 V	LiTFSI in an aprotic electrolyte	[90]
O_2	Lattice oxygen of cathode	High cathode potential	$\geq$~4.3 V	NMC//Li, $LiPF_6$ in EC/EMC	[43a]

*No experimental data is found.

gases twice from a pouch cell during the whole charging process (~30 hours).[30] In this regard, the gas dynamics are nearly absent during cycling, such that the possible gas consumption and cross-talks can hardly be tracked. Like VSGA, this apparatus can only monitor the gas volume change but can hardly track the gas evolution processes in situ.

4.3. Gas Consumption in DEMS

One of the intrinsic shortcomings of the DEMS technique is that the events of gas consumption cannot be tracked since the gasses are already stripped out. Multiple studies have highlighted the gas consumption in LIBs using other experimental methods. Aiken et al. observed that the gases formed after the first charge are slowly consumed during the subsequent cycles.[25] Later, the same group also found that the charged NMC cells also consume gases during storage.[27] For instance, a clear gas consumption was observed by Ellis et al. that over 40% of the gases generated after the initial charge of an NMC cell are consumed within the first 100 hours of storage at 40 °C. In the same study, the authors also discovered that different SoCs may lead to gas consumption at different rates.[30]

4.4. Unstable Pressure of OEMS

The OEMS system illustrated in Figure 4 partly mitigates the drawbacks of DEMS. With a capillary to collect the evolved gases, both the carrier gas and dehumidifier of DEMS are no longer necessary, such that the risk of electrolyte drying is largely mitigated. Other components of both techniques remain almost the same owing to the similar working principle, i.e., a designated cell with a sophisticated mass spectrometer. In other words, OEMS is also designed primarily for research purposes, especially since leaking in commercial rechargeable batteries can hardly be acceptable. Moreover, continuous sampling may lead to a non-constant internal pressure because different gassing events would occur at different time points while the sampling capillary is leaking at a constant rate. The semi-closed OEMS setup constructed by Berg et al. stands out since it can maintain a semi-constant internal pressure of the cell by repeated Ar re-filling and being compatible with large-format cells through a homemade adaptor/casing.[19,23b]

4.5. Application and Research Concerns

Overall, the currently available technologies presented in this review are all primarily developed for research purposes, and thus remaining on lab scales. Both DEMS and OEMS techniques have made significant progress in the field of battery gas sensing and have greatly enhanced our understanding of the physical and chemical processes inside rechargeable batteries. Thanks to the powerfulness of MS or GC technique, high-precision quantitative data that possess rich scientific information are collected. Subsequent analyses would undoubtedly help unlock various chemical events inside battery cells. These technologies, on the other hand, have some drawbacks as well: (1) These mass spectrometer systems are often, large, complex, and expensive; (2) MS sampling will affect the battery, making the detection conditions unexpectedly deviate from the actual working conditions; (3) Due to the issues like electrolyte dry-out or gas pressure change, continuous testing on a long-term basis can be challenging; (4) Volatile organic molecules from the electrolyte solvents may enter the mass spectrometer, resulting in gas fragments during ionization that may affect the measurement accuracy; (5) Gas inlet and outlet valves are required, so most of the current work is still limited to specific cell molds (e.g., designated Swagelok parts), which deviate from the commercial designs.[39]

Therefore, operando gas sensing for commercial batteries is quite challenging. An adaptable gas sensing technology is of vital importance for smarter and safer use of rechargeable batteries in various applications. In this way, not only does the technology advance the battery field, but it could also be extended to other energy storage devices. When considering application merits, one should revisit whether the versatility of the MS or GC is necessary. For example, H_2 evolution is believed to primarily originate from residue moisture in the electrode and electrolyte. Water contamination can then be revealed by tracking H_2 alone. Likewise, CO_2 is often observed at high cell voltage, i.e., high cathode potentials, which triggers oxidation reactions. Consequently, the CO_2 concentration inside can be used to tell whether a cell is unexpectedly overcharged. These two examples suggest that monitoring one or two gas types may potentially be sufficient for certain purposes.

In the sector of research and development, high-capacity electrodes are always needed to boost the cell-level energy density of LIBs. While many alloy anodes exhibit significantly higher theoretical capacities than the current state-of-the-art graphite, such as silicon,[95] tin,[96] and aluminum,[97] improving the capacity of cathode materials is more challenging due to their intercalation chemistry. Many efforts can be found in developing and understanding the high-capacity cathode materials, during which gas evolution is often observed.[80b,87d,98] Moving to post Li storage technologies, sodium-ion batteries (SIBs) are known to share similar chemistries (e.g., same electrolyte solvents) with LIBs, their gassing behaviors should not be distinctively different.[99] To largely mitigate the dendrite issue, all solid-state batteries (ASSBs) attracted lots of attention in recent years, which are also found to exhibit different gassing behaviors. For example, SO_2 evolution is observed in solid-state Li-ion cells, indicating solid electrolyte decomposition (lithium thiophosphate-based) that further triggers the formation of oxidized phosphorus and sulfur species.[100] Cumulatively, other energy storage systems in addition to the well-established LIB chemistry, e.g., aqueous-based, such as aqueous batteries and supercapacitors, often use acid/base or salts dissolved in water.[101] In this particular case, H_2 and O_2 are of vital importance since unwanted water splitting is one of the main reasons that is responsible for coulombic inefficiencies in aqueous cells. For example, Ma et al. assembled an aqueous Zn-metal battery that maintained nearly 100% coulombic effi-

ciency after 100 cycles by suppressing H_2 evolution and O_2-induced Zn corrosion.[102] Also, He et al. used the OEMS technique to successfully detect H_2 on the anode at a cell voltage higher than 1.6 V due to water splitting and CO on the cathode due to carbon corrosion, which correlates with the cell aging phenomena.[101b] These studies highlight the importance of operando gas sensing on fundamental understandings in energy storage devices other than LIBs.

5. Optical Fiber-Based Sensing Technologies

As people have increasingly realized the importance of battery sensing at a cell level, which can involve the mechanics, kinetics, and dynamics of the solid-liquid and solid-solid interfaces, efforts have been made to develop appropriate sensing technologies for (commercial) rechargeable batteries. Ideally, new technology should be non-destructive, low cost, durable, and easy to implement. Integrating optical fiber sensors (e.g., fiber Bragg grating; FBG) onto or into battery cells seems a promising solution due to their size, flexibility, transmission speed, and electromagnetic resistance, offering great opportunities in cell-, pack-, and module-level tests.[103] Thanks to the long history of optical fiber sensing, the technology has exhibited its capability in temperature/strain/pressure measurement, and more recently gas sensing.[104] This section discusses the recent progress of optical fiber sensors in the field of battery monitoring, following a sequence from the external and to the internal temperature/strain/pressure sensing. As such, the future trend of optical fiber-based gas sensing for rechargeable batteries is also projected at the end of this chapter.

5.1. External Temperature and Strain Measurements

Leitão et al.[105] and Yang et al.[106] were perhaps the first ones who introduce FBG sensors into the field of rechargeable batteries just over ten years ago. In brief, the changes in temperature and strain would modify the period of FBG, leading to a shift in the resonance of the FBG and hence the reflected wavelength (Figure 11a). The thermal behavior inside the batteries can be recorded by FBG sensors affixed on the cell package, regardless of whether the batteries are being operated under normal or abnormal conditions.[106] The technology was also extended to explore the intercalation stages of LIBs, showcasing its high accuracy towards temperature and strain measurements. The obtained data were also double checked with independent means, i.e., electric strain gauge and thermistor, as shown in Figure 11b.[103] Recently, Bonefacino and Ghashghaie et al. further optimized the technique using FBG inscribed in a polymer fiber (POF; Figure 11c), which has significantly higher thermal (negative slope; Figure 11d) and strain (positive slope; Figure 11e) coefficients than silica fiber, thus enabling even higher sensitivities. By coupling POF-FBG with silica-FBG, high-fidelity operando monitoring of rechargeable batteries is achieved using externally fitted optical fiber sensors.[21c]

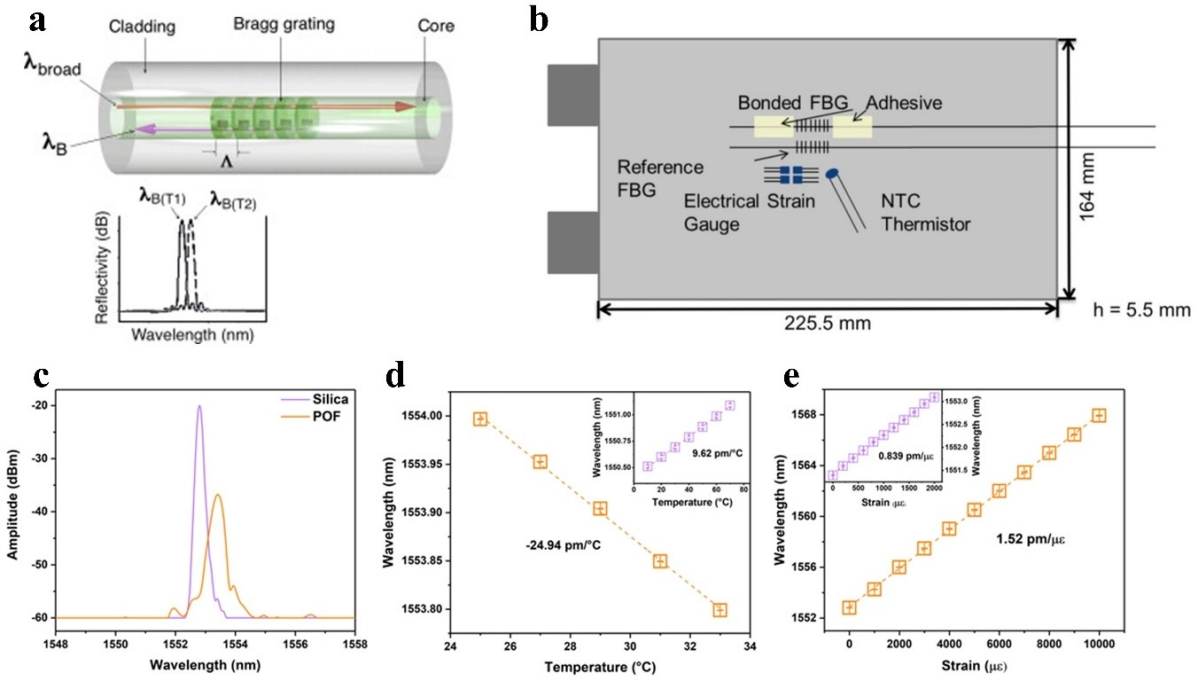

Figure 11. (a) Schematic of an optical fiber with an FBG. The reflected spectrum shows a shift due to temperature variation (T1 < T2). λ_{broad}: Incident light; λ_B: reflected light. Reprinted with permission 2013 Elsevier B. V.[106] (b) Schematic of the experimental setup for monitoring strain and temperature of Li-Ion pouch cells by FBG sensors. A bonded FBG sensor is attached to the cell package with an adhesive to monitor strain and temperature. Reference FBG sensor is loosely placed on the cell package with heat conducting paste. Reprinted with permission 2015 IOP Ltd.[103] (c) POF and SMF FBG spectra. (d) Thermal sensitivity of the POF and SMF (inset). (e) Strain sensitivity of the POF and SMF (inset). Reprinted with permission 2022 CC BY NC ND 4.0.[21c]

In short, the external sensors can generate unique data, which may be particularly beneficial for cell assessments, as opposed to solely relying on coulombic monitoring. Naturally, more sophisticated analyses can be expected by establishing correlations between the performance indicators and the sensing data.

5.2. Internal Temperature and Pressure Measurements

While external monitoring offers a simple, straightforward, and cost-effective sensing solution for real-time battery assessment, internal monitoring remains essential for unlocking the battery chemistry and harvesting information from the inside. In 2020, Huang et al. placed optical fiber sensors into an 18650 cylindrical Na-ion cell. With a silica-FBG and a micro-structured hollow-core fiber (MS-HCF), the internal temperature and pressure were successfully decoded in real-time with high accuracy.[17] Since then, more efforts of optical fiber-based sensing have been put into the field of rechargeable batteries. Guo and team have integrated a Fabry–Perot interferometer (FPI) with an FBG in a cascade structure, making it possible to simultaneously monitor temperature and pressure inside batteries for thermal runaway using a single fiber. The working principle is schematically explained in Figure 12.[12]

Moreover, Huang et al. utilized the tilted FBG to study the electrolyte chemistry. By rotating the FBG's grating plane with a certain angle perpendicular to the fiber axis, a larger number of backward-propagating cladding modes can be created in addition to a single forward-propagating core mode. These cladding mode resonances can interact with and be affected by the surroundings, e.g., electrolytes in batteries. The data harvested by tilted FBG were found to be strongly correlated to the capacity loss.[21d] Differently, Gervillié-Mouravieff et al. introduced evanescent wave infrared spectroscopy using benign chalcogenide fibers inside the Swagelok cells, particularly for monitoring the stability of electrolyte components in real-time.[21b]

Successfully integrating optical fiber sensors into battery cells is expected to offer relevant information for numerous purposes. The effort could potentially generate insights into various components of rechargeable batteries, such as SEI[17] and electrolytes.[21d] Moreover, the strain/stress sensitivity of the sensors could advance the understanding of state-of-the-art electrodes[107] and the development of new electrodes[108] since their volume changes and associated mechanical stresses are known to be problematic. Indeed, the ability to decouple gas generation from solid mechanics is a priority, considering that FBG signals also capture information from gas evolution, e.g., gas pressure.

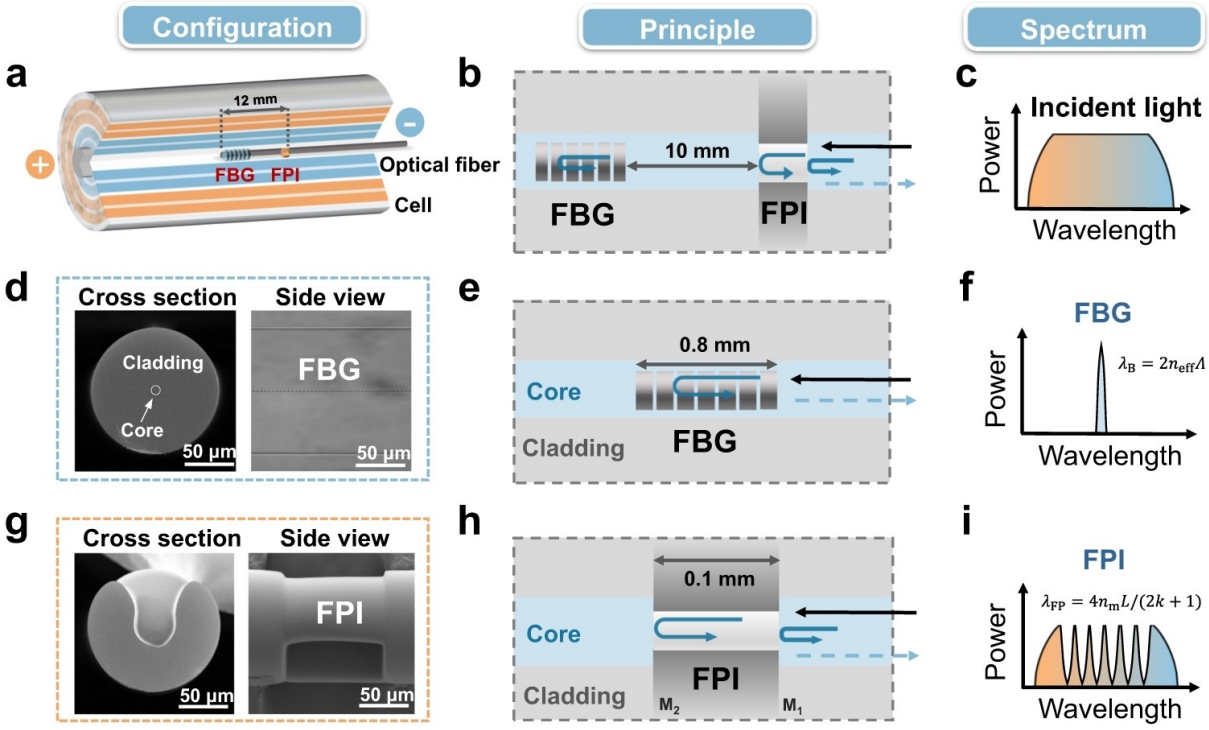

Figure 12. Principle of combined FBG/FPI sensor for simultaneous temperature and pressure monitoring in the cell. (a) The position of the sensor in the battery. (b) The cascade structure of FBG-FPI sensor. (c) the incident broadband light spectrum. (d) Cross-section image (left) and the side view (right) of the fabricated FBG. (e) and (f) Diagrams of the sensing principle of FBG. FBG reflects particular wavelengths of incident light and transmits all others, which is determined by the periodic variation in the refractive index (RI) of the FBG. (g) The FPI configuration (left: cross-section, right: side view). (h) and (i) Diagrams of the sensing principle of FPI. The two fiber end-faces (M1 and M2) reflect the incident light. The two reflected beams interfere, resulting in a periodic fringe pattern in the spectrum and enabling the detection of the phase difference between the two reflected beams. Reprinted with permission 2023 CC BY 4.0.[12]

5.3. Emerging Gas Sensing Technologies

Laser spectroscopy is a powerful technology offering gas detection with great sensitivity and specificity.[109] Among different techniques of lase spectroscopy, laser absorption spectroscopy (LAS) relies on the "fingerprint"-like absorption wavelengths of gas molecules. Traditional laser spectroscopic system for gas detection employs discrete free-space optical components, which are bulky and not suitable for space-limited applications, e.g., operando gas detection in battery cells. The newly developed MS-HCF has been proven to be an efficient platform for light-gas interactions.[110] MS-HCF has an outer diameter of hundreds of micrometers, making the sensors compact and flexible. Attempts have been made to construct an all-fiber gas cell with MS-HCF which allows gas detection with compact sensing elements and easy integration with optical fiber systems.[111] Optical gas sensors with LAS have been demonstrated using MS-HCF gas cells with noise equivalent concentration (NEC) of a few parts-per-million (ppm) for gases with relatively strong absorptions, e.g., CH_4 and C_2H_2. [112]

Photothermal spectroscopy (PTS) is a derivative of LAS, which captures the optical phase modulation results from the gas absorptions. A pump-probe configuration is typically adopted for PTS gas detection. A pump beam is periodically modulated in intensity or wavelength as its nominal wavelength is tuned to the center of absorption lines of the targeted gas molecules (e.g., C_2H_4). Gas molecules absorb pump power and generate heat via thermal relaxation, which modulates the temperature and hence, the RI of gases.[113] The probe beam is used to detect the accumulated optical phase modulation with its wavelength away from the gas absorption lines. Recently, MS-HCF has been adopted to enhance the photothermal effect, which significantly improves the gas detection limit. MS-HCF can strongly confine the optical mode within the hollow core area with a mode diameter $<50\ \mu m$, which greatly increases the light intensity and enhances interactions between light and gas molecules compared with free-space optical systems.[114] In 2015, Jin et al. reported the first demonstration of C_2H_2 detection with NEC down to 2 parts-per-billion (ppb) and an unprecedentedly large dynamic range of 5 orders of magnitude using a fiber Mach-Zehnder photothermal interferometer (PTI) with a 10-meter long MS-HCF.[104] The performance of the PTS gas sensors can be substantially improved by the deployment of a mode-phase-difference PTI using the MS-HCF that can support dual transverse modes, i.e., the LP_{01} and LP_{11} modes. The detection of mode-phase-difference has better resistance to external disturbance than the detection of the fundamental mode phase, which enables a significantly higher signal-to-noise ratio, and thus very sensitive gas detection with NEC on the level of parts-per-trillion (ppt) using 5-meter long MS-HCF.[115]

A simpler and more compact configuration of PTS gas sensors is based on the FPI. The FPI may be constructed by connecting the MS-HCF with two pieces of single-mode fiber (SMF) which have flat end faces with 4% reflections. The reflected waves at the interfaces between the HCF and the SMF interfere, allowing the detection of the phase difference between the two reflected beams. For a typical FPI configuration shown in Figure 13, the probe beams reflected by the two interfaces generally have a short time delay of ≤ 1 ns for an MS-HCF length of ≤ 15 cm. Environmental disturbance with low frequency imposed on the sensor would affect the phases of the reflected beams in a similar way which may be cancelled out and has little influence on the gas detection.[116] With the probe wavelength near 1550 nm and the pump wavelength ranging from 760 nm to 4.6 μm, the detections of O_2,[117] C_2H_2,[116] NH_3,[118] CH_4,[118] C_2H_6,[119] CO,[120] and CO_2,[120] have been demonstrated with NEC down to ppm and ppb levels with fast response. It should be noted that the detection limit of the MS-FPI gas sensors is determined by the noise of the interrogation system, which holds true for almost all kinds of optical gas sensing technologies. The design of the sensor does not restrict the lowest gas concentrations being detected. More recently, the developed low-coherence PTI gas sensor uses the low-coherent probe to suppress parasitic interference and improve the measurement precision as well as the long-term stability of gas detection. C_2H_2 detection with NEC of 0.7 ppb and measurement precision of 0.025% are realized. The instability of the detection over a period of 3 hours is ± 0.038%, ten times better than the state-of-the-art PTS.[121] The detection limit can be further improved down to the ppt level by using a resonant FP cavity, providing new opportunities for operando gas sensing in rechargeable batteries.[122] It is believed that the technology also holds potential for being used in other energy storage devices, such as supercapacitors, electrolyzers, and fuel cells.[123]

Table 3 compares the different technologies in terms of their pros and cons, and provides an overview of each gas sensing technique, which allows people to assess their

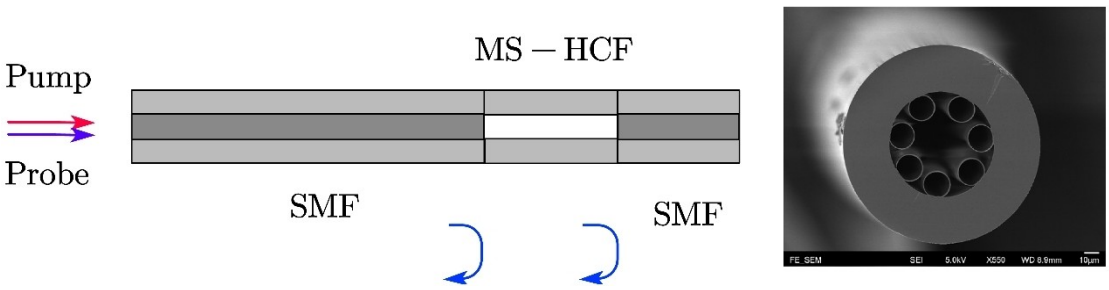

Figure 13. Schematic illustration of the MS-HCF FPI gas sensor, together with the cross-sectional SEM image of the anti-resonant HCF. Reprinted with permission 2020 CC BY.[116]

Table 3. Comparisons of various gas sensing techniques that are (or will possibly be) applied in the field of electrochemical energy storage.

Technique	Essential components	Battery compatibility	Test capacity	Strengths	Limitations
VGSA	Specially designed cell, gas-tight syringe, Pressure transducer	Compact, incompatible with commercial cells	One cell	Quick volume quantification	No gas qualification
AISGA	Pouch cell, immersing liquid, home-made balance, gas chromatographer	Bulky, compatible with pouch cells	One cell	*In situ* volume monitoring	Limited gas qualification
DEMS	Stripping gas flow, specially designed cell, mass spectrometer	Bulky, incompatible with commercial cells	One cell	*Operando*, high precision, versatility	Gas consumption undetectable
OEMS	Specially designed cell, capillary leakage, mass spectrometer	Bulky, compact, incompatible with commercial cells	One cell or Multiple cells	*Operando*, high precision, versatility	Unstable internal pressure
MS-PTS*	Optical fiber, photo-thermal gas analyzer	Compact, compatible with commercial cells	Multiple cells	*Operando*, high precision, high selectivity	Gases with low photo-thermal absorption
ELC Sensor	Electrodes, Electrolyte, Membrane	Compact, compatible with commercial cells	One cell	*Operando*, high precision	Corrosion, cross-sensitivity, low dynamic range
NDIR Sensor	Broadband lamp source, optical filter, IR detector	Bulky, incompatible with commercial cells	One cell	*Operando*, high selectivity	Low sensitivity, interference No experimental demonstration yet.

*No experimental demonstration yet.

commercialization potentials in the field of battery gas sensing when application standards are considered. In addition to the gas sensing technologies presented before, conventional electrochemical (ELC)[124] and nondispersive infrared (NDIR)[125] gas sensors which seem to exhibit potential in the field of battery sensing, are also included in the comparison. Among them, MS-HCF FPI exhibits some unique features for battery sensing, such as its compatibility with commercial cells and simultaneous test capabilities of multiple cells. Although the MS-HCF FPI gas sensing for rechargeable batteries is still under development on a lab scale, it seems to exhibit great potential for academic research and commercial applications considering the success in fiber-based strain/pressure sensing for batteries in recent years.[1,12,21b,d,126]

6. Summary and Outlook

Real-time sensing is a promising way to make future battery products more reliable and sustainable. Current technologies rely on supplemental information from electrochemistry to estimate crucial indicators like SoC, SoP, and SoH of rechargeable batteries. Although fairly accurate estimates can be achieved with the assistance of mathematic models, catastrophic incidents almost seem inevitable as seen in day-to-day news. Efforts have been made to directly monitor physical factors, such as temperature and strain at a package level, which are closely associated with cell conditions. Recently, great progress has been made in optical fiber-based sensing for measuring the temperature and pressure of battery cells from inside, such that important associated chemical and thermal events can be decoded in real-time with high accuracy. These factors, however, may be secondary if considering specific (electro−) chemical reactions occurring at electrode/electrolyte interfaces. In this regard, gaseous species are suggested to be the 'fingerprint', which could directly reveal the chemical reactions inside batteries during charge and discharge. By deploying sophisticated experimental apparatus, scientists managed to conduct research on gas evolution in LIBs and have highlighted the importance of H_2, C_2H_4, CO, CO_2, and O_2. We hope that the scientific contents of this review could serve as a baseline for people who are seeking a better understanding of the gassing chemistries in LIBs.

Looking forward, while recognizing the importance of operando gas sensing for rechargeable batteries, the currently available apparatuses appear to lack technical and financial feasibility for scaling to cell levels in applications (e.g., EVs or stationary power systems). Facile and cost-effective gas sensing technologies are therefore necessary for the future utilization of chemistry-specific information. However, this field, so far, is still quite empty, such that extra efforts should be put into establishing new multi-/inter-disciplinary research topics that could help tackle the difficulties. We believe that fiber-based LAS can be promising candidates in this regard, especially since FBG sensors with a similar geometry have shown great successes in temperature, strain, and pressure sensing recently. As compared to free space, MS-HCF LAS exhibits numerous advantages, such as small size, high flexibility, and simple light alignment. Through manipulating the wavelength of the light, specific gaseous species can be detected with high precision and fast response. Importantly, depending on various application purposes, this technology can enable either a multi-component gas measurement with a wide range, or a single gas monitoring with a high selectivity. Not only does the technology offer great opportunities for operando gas sensing

in Li-/Na-ion batteries, but it could also potentially be extended to monitor other energy storage devices.

Acknowledgments

T. Zheng is supported by the "PolyU Distinguished Postdoctoral Fellowship Scheme" (1-YWBT) at The Hong Kong Polytechnic University (PolyU). M. Muneeswara acknowledges the Centre for Advances in Reliability and Safety (CAiRS) admitted under AIR@InnoHK Research Cluster. H. Bao would like to acknowledge the project (1-BDSP) at Poly U. S. T. Boles acknowledges the ENERSENSE research initiative (68024013) at Norwegian University of Science and Technology (NTNU), Norway.

Conflict of Interests

The authors declare no conflict of interest.

Data Availability Statement

The data that support the findings of this study are available from the corresponding author upon reasonable request.

Keywords: Operando monitoring · Optical fiber sensor · Photothermal spectroscopy · Rechargeable batteries · Sensing technologies

[1] J. Huang, S. T. Boles, J.-M. Tarascon, *Nature Sustainability* **2022**, *5*, 194–204.
[2] C. P. Grey, D. S. Hall, *Nat. Commun.* **2020**, *11*, 6279.
[3] R. C. Lanphier, *Transactions (Society of Automobile Engineers)* **1911**, *6*, 371–393.
[4] J. A. Mas, *Battery charging system and transducer therefor*, Google Patents, **1969**, 3460019.
[5] M. Keddam, Z. Stoynov, H. Takenouti, *J. Appl. Electrochem.* **1977**, *7*, 539–544.
[6] D. D. Macdonald, *Electrochim. Acta* **2006**, *51*, 1376–1388.
[7] a) I. Bloom, A. N. Jansen, D. P. Abraham, J. Knuth, S. A. Jones, V. S. Battaglia, G. L. Henriksen, *J. Power Sources* **2005**, *139*, 295–303; b) I. Bloom, J. Christophersen, K. Gering, *J. Power Sources* **2005**, *139*, 304–313; c) I. Bloom, J. P. Christophersen, D. P. Abraham, K. L. Gering, *J. Power Sources* **2006**, *157*, 537–542; d) I. Bloom, L. K. Walker, J. K. Basco, D. P. Abraham, J. P. Christophersen, C. D. Ho, *J. Power Sources* **2010**, *195*, 877–882.
[8] H. M. Dahn, A. J. Smith, J. C. Burns, D. A. Stevens, J. R. Dahn, *J. Electrochem. Soc.* **2012**, *159*, A1405.
[9] a) I. D. Campbell, M. Marzook, M. Marinescu, G. J. Offer, *J. Electrochem. Soc.* **2019**, *166*, A725; b) W. M. Dose, J. K. Morzy, A. Mahadevegowda, C. Ducati, C. P. Grey, M. F. L. De Volder, *J. Mater. Chem. A* **2021**, *9*, 23582–23596.
[10] a) J. Li, M. Zhao, C. Dai, Z. Wang, M. Pecht, *J. Electroanal. Chem.* **2021**, *895*, 115488; b) S. Amir, M. Gulzar, M. O. Tarar, I. H. Naqvi, N. A. Zaffar, M. G. Pecht, *IEEE Access* **2022**, *10*, 18279–18288; c) S. Peng, A. Zhang, D. Liu, M. Cheng, J. Kan, M. Pecht, *State-of-Charge Estimation of Lithium-Ion Batteries Based on Dual-Coefficient Tracking Improved Square-Root Unscented Kalman Filter, Vol. 9* **2023**; d) J. P. Schmidt, D. Manka, D. Klotz, E. Ivers-Tiffée, *J. Power Sources* **2011**, *196*, 8140–8146; e) B. Liebhart, L. Komsiyska, C. Endisch, *J. Power Sources* **2020**, *449*, 227297.
[11] M. Armand, J. M. Tarascon, *Nature* **2008**, *451*, 652–657.
[12] W. Mei, Z. Liu, C. Wang, C. Wu, Y. Liu, P. Liu, X. Xia, X. Xue, X. Han, J. Sun, G. Xiao, H.-y. Tam, J. Albert, Q. Wang, T. Guo, *Nat. Commun.* **2023**, *14*, 5251.
[13] T. Amietszajew, J. Fleming, A. J. Roberts, W. D. Widanage, D. Greenwood, M. D. R. Kok, M. Pham, D. J. L. Brett, P. R. Shearing, R. Bhagat, *Batteries & Supercaps* **2019**, *2*, 934–940.
[14] C. Forgez, D. Vinh Do, G. Friedrich, M. Morcrette, C. Delacourt, *J. Power Sources* **2010**, *195*, 2961–2968.
[15] A. Knobloch, C. Kapusta, J. Karp, Y. Plotnikov, J. B. Siegel, A. G. Stefanopoulou, *J. Electron. Packag.* **2018**, *140*, 031002.
[16] J. O. Majasan, J. B. Robinson, R. E. Owen, M. Maier, A. N. P. Radhakrishnan, M. Pham, T. G. Tranter, Y. Zhang, P. R. Shearing, D. J. L. Brett, *Journal of Physics: Energy* **2021**, *3*, 032011.
[17] J. Huang, L. Albero Blanquer, J. Bonefacino, E. R. Logan, D. Alves Dalla Corte, C. Delacourt, B. M. Gallant, S. T. Boles, J. R. Dahn, H.-Y. Tam, J.-M. Tarascon, *Nat. Energy* **2020**, *5*, 674–683.
[18] K. Mc Carthy, H. Gullapalli, T. Kennedy, *J. Power Sources* **2022**, *519*, 230786.
[19] R. Lundström, E. J. Berg, *J. Power Sources* **2021**, *485*, 229347.
[20] S. Zhu, L. Yang, J. Wen, X. Feng, P. Zhou, F. Xie, J. Zhou, Y.-N. Wang, *J. Power Sources* **2021**, *516*, 230669.
[21] a) K. Tan, W. Li, Z. Lin, X. Han, X. Dai, S. Li, Z. Liu, H. Liu, L. Sun, J. Jiang, T. Liu, K. Wu, T. Guo, S. Wang, *J. Power Sources* **2023**, *580*, 233471; b) C. Gervillié-Mouravieff, C. Boussard-Plédel, J. Huang, C. Leau, L. A. Blanquer, M. B. Yahia, M. L. Doublet, S. T. Boles, X. H. Zhang, J. L. Adam, J. M. Tarascon, *Nat. Energy* **2022**, *7*, 1157–1169; c) J. Bonefacino, S. Ghashghaie, T. Zheng, C.-P. Lin, W. Zheng, L. A. Blanquer, J. Huang, C. Gervillié, H.-Y. Tam, J.-M. Tarascon, S. T. Boles, *J. Electrochem. Soc.* **2022**, *169*, 100508; d) J. Huang, X. Han, F. Liu, C. Gervillié, L. A. Blanquer, T. Guo, J.-M. Tarascon, *Energy Environ. Sci.* **2021**, *14*, 6464–6475; e) S. Y. Han, C. Lee, J. A. Lewis, D. Yeh, Y. Liu, H.-W. Lee, M. T. McDowell, *Joule* **2021**; f) B. Özdogru, H. Dykes, S. Padwal, S. Harimkar, Ö. Ö. Çapraz, *Electrochim. Acta* **2020**, *353*, 136594; g) W. Zhang, D. Schröder, T. Arlt, I. Manke, R. Koerver, R. Pinedo, D. A. Weber, J. Sann, W. G. Zeier, J. Janek, *J. Mater. Chem. A* **2017**, *5*, 9929–9936; h) A. J. Louli, L. D. Ellis, J. R. Dahn, *Joule* **2019**, *3*, 745–761.
[22] B. B. Berkes, A. Jozwiuk, M. Vračar, H. Sommer, T. Brezesinski, J. Janek, *Anal. Chem.* **2015**, *87*, 5878–5883.
[23] a) U. Mattinen, M. Klett, G. Lindbergh, R. Wreland Lindström, *J. Power Sources* **2020**, *477*, 228968; b) C. Misiewicz, R. Lundström, I. Ahmed, M. J. Lacey, W. R. Brant, E. J. Berg, *J. Power Sources* **2023**, *554*, 232318.
[24] R. Fong, M. C. Reid, R. S. McMillan, J. R. Dahn, *J. Electrochem. Soc.* **1987**, *134*, 516.
[25] C. P. Aiken, J. Xia, D. Y. Wang, D. A. Stevens, S. Trussler, J. R. Dahn, *J. Electrochem. Soc.* **2014**, *161*, A1548.
[26] J. Self, C. P. Aiken, R. Petibon, J. R. Dahn, *J. Electrochem. Soc.* **2015**, *162*, A796.
[27] C. P. Aiken, J. Self, R. Petibon, X. Xia, J. M. Paulsen, J. R. Dahn, *J. Electrochem. Soc.* **2015**, *162*, A760.
[28] D. J. Xiong, R. Petibon, M. Nie, L. Ma, J. Xia, J. R. Dahn, *J. Electrochem. Soc.* **2016**, *163*, A546.
[29] D. J. Xiong, L. D. Ellis, R. Petibon, T. Hynes, Q. Q. Liu, J. R. Dahn, *J. Electrochem. Soc.* **2016**, *164*, A340–A347.
[30] L. D. Ellis, J. P. Allen, L. M. Thompson, J. E. Harlow, W. J. Stone, I. G. Hill, J. R. Dahn, *J. Electrochem. Soc.* **2017**, *164*, A3518.
[31] a) X. Ma, J. E. Harlow, J. Li, L. Ma, D. S. Hall, S. Buteau, M. Genovese, M. Cormier, J. R. Dahn, *J. Electrochem. Soc.* **2019**, *166*, A711; b) R. Gauthier, D. S. Hall, T. Taskovic, J. R. Dahn, *J. Electrochem. Soc.* **2019**, *166*, A3707.
[32] J. E. Harlow, X. Ma, J. Li, E. Logan, Y. Liu, N. Zhang, L. Ma, S. L. Glazier, M. M. E. Cormier, M. Genovese, S. Buteau, A. Cameron, J. E. Stark, J. R. Dahn, *J. Electrochem. Soc.* **2019**, *166*, A3031.
[33] a) D. S. Hall, M. Nie, L. D. Ellis, S. L. Glazier, S. Hyatt, R. Petibon, A. Xiao, W. M. Lamanna, K. Smith, I. G. Hill, J. R. Dahn, *J. Electrochem. Soc.* **2016**, *163*, A773; b) D. S. Hall, J. P. Allen, S. L. Glazier, L. D. Ellis, L. Ma, J. M. Peters, I. G. Hill, J. R. Dahn, *J. Electrochem. Soc.* **2017**, *164*, A3445.
[34] R. Imhof, P. Novák, *J. Electrochem. Soc.* **1998**, *145*, 1081.
[35] P. Novák, D. Goers, L. Hardwick, M. Holzapfel, W. Scheifele, J. Ufheil, A. Würsig, *J. Power Sources* **2005**, *146*, 15–20.
[36] A. Schiele, H. Sommer, T. Brezesinski, J. Janek, B. Berkes, *Reference Module in Chemistry, Molecular Sciences and Chemical Engineering*, Elsevier, **2017**.
[37] B. B. Berkes, A. Jozwiuk, H. Sommer, T. Brezesinski, J. Janek, *Electrochem. Commun.* **2015**, *60*, 64–69.
[38] N. Tsiouvaras, S. Meini, I. Buchberger, H. A. Gasteiger, *J. Electrochem. Soc.* **2013**, *160*, A471.

[39] R. Bernhard, S. Meini, H. A. Gasteiger, *J. Electrochem. Soc.* **2014**, *161*, A497–A505.
[40] R. Bernhard, M. Metzger, H. A. Gasteiger, *J. Electrochem. Soc.* **2015**, *162*, A1984–A1989.
[41] M. Metzger, C. Marino, J. Sicklinger, D. Haering, H. A. Gasteiger, *J. Electrochem. Soc.* **2015**, *162*, A1123.
[42] M. Metzger, B. Strehle, S. Solchenbach, H. A. Gasteiger, *J. Electrochem. Soc.* **2016**, *163*, A798–A809.
[43] a) R. Jung, M. Metzger, F. Maglia, C. Stinner, H. A. Gasteiger, *J. Electrochem. Soc.* **2017**, *164*, A1361; b) R. Jung, P. Strobl, F. Maglia, C. Stinner, H. A. Gasteiger, *J. Electrochem. Soc.* **2018**, *165*, A2869–A2879.
[44] L. A. Kaufman, T.-Y. Huang, D. Lee, B. D. McCloskey, *ACS Appl. Mater. Interfaces* **2022**, *14*, 39959–39964.
[45] S. E. Renfrew, L. A. Kaufman, B. D. McCloskey, *ACS Appl. Mater. Interfaces* **2019**, *11*, 34913–34921.
[46] a) B. L. D. Rinkel, D. S. Hall, I. Temprano, C. P. Grey, *J. Am. Chem. Soc.* **2020**, *142*, 15058–15074; b) B. L. D. Rinkel, J. P. Vivek, N. Garcia-Araez, C. P. Grey, *Energy Environ. Sci.* **2022**, *15*, 3416–3438.
[47] a) I. Belharouak, G. M. Koenig, K. Amine, *J. Power Sources* **2011**, *196*, 10344–10350; b) I. Belharouak, G. M. Koenig, T. Tan, H. Yumoto, N. Ota, K. Amine, *J. Electrochem. Soc.* **2012**, *159*, A1165–A1170.
[48] S. C. Weiner, L. L. Fassbender, K. A. Quick, *Int. J. Hydrog. Energy* **2011**, *36*, 2729–2735.
[49] D. J. Xiong, R. Petibon, L. Madec, D. S. Hall, J. R. Dahn, *J. Electrochem. Soc.* **2016**, *163*, A1678.
[50] J. C. Burns, N. N. Sinha, G. Jain, H. Ye, C. M. VanElzen, E. Scott, A. Xiao, W. M. Lamanna, J. R. Dahn, *J. Electrochem. Soc.* **2014**, *161*, A247.
[51] J. C. Burns, N. N. Sinha, G. Jain, H. Ye, C. M. VanElzen, E. Scott, A. Xiao, W. M. Lamanna, J. R. Dahn, *J. Electrochem. Soc.* **2013**, *160*, A2281.
[52] J. Hoffmann, M. S. Milien, B. L. Lucht, M. Payne, *J. Electrochem. Soc.* **2018**, *165*, A3108.
[53] R. Jung, R. Morasch, P. Karayaylali, K. Phillips, F. Maglia, C. Stinner, Y. Shao-Horn, H. A. Gasteiger, *J. Electrochem. Soc.* **2018**, *165*, A132.
[54] a) Y.-B. He, B. Li, M. Liu, C. Zhang, W. Lv, C. Yang, J. Li, H. Du, B. Zhang, Q.-H. Yang, J.-K. Kim, F. Kang, *Sci. Rep.* **2012**, *2*, 913; b) K. Wu, J. Yang, Y. Liu, Y. Zhang, C. Wang, J. Xu, F. Ning, D. Wang, *J. Power Sources* **2013**, *237*, 285–290.
[55] M. Holzapfel, F. Alloin, R. Yazami, *Electrochim. Acta* **2004**, *49*, 581–589.
[56] C. R. Fell, L. Sun, P. B. Hallac, B. Metz, B. Sisk, *J. Electrochem. Soc.* **2015**, *162*, A1916–A1920.
[57] D. Aurbach, M. Daroux, P. Faguy, E. Yeager, *J. Electroanal. Chem. Interfacial Electrochem.* **1991**, *297*, 225–244.
[58] T. Zheng, S. T. Boles, *Progress in Energy* **2023**, *5*, 032001.
[59] T. Ohzuku, A. Ueda, N. Yamamoto, *J. Electrochem. Soc.* **1995**, *142*, 1431.
[60] B. Rowden, N. Garcia-Araez, *Energy Reports* **2020**, *6*, 10–18.
[61] M. He, E. Castel, A. Laumann, G. Nuspl, P. Novák, E. J. Berg, *J. Electrochem. Soc.* **2015**, *162*, A870–A876.
[62] A. Schiele, T. Hatsukade, B. B. Berkes, P. Hartmann, T. Brezesinski, J. Janek, *Anal. Chem.* **2017**, *89*, 8122–8128.
[63] A. Schechter, D. Aurbach, H. Cohen, *Langmuir* **1999**, *15*, 3334–3342.
[64] a) D. Strmcnik, I. E. Castelli, J. G. Connell, D. Haering, M. Zorko, P. Martins, P. P. Lopes, B. Genorio, T. Østergaard, H. A. Gasteiger, F. Maglia, B. K. Antonopoulos, V. R. Stamenkovic, J. Rossmeisl, N. M. Markovic, *Nature Catalysis* **2018**, *1*, 255–262; b) T. Melin, R. Lundström, E. J. Berg, *Adv. Mater. Interfaces* **2022**, *9*, 2101258.
[65] S. Solchenbach, M. Metzger, M. Egawa, H. Beyer, H. A. Gasteiger, *J. Electrochem. Soc.* **2018**, *165*, A3022.
[66] F. Jeschull, L. Zhang, Ł. Kondracki, F. Scott, S. Trabesinger, *Journal of Physics: Energy* **2023**, *5*, 025003.
[67] B. Michalak, B. B. Berkes, H. Sommer, T. Brezesinski, J. Janek, *J. Phys. Chem. C* **2017**, *121*, 211–216.
[68] N. E Galushkin, N. N. Yazvinskaya, D. N. Galushkin, *J. Electrochem. Soc.* **2019**, *166*, A897.
[69] a) M. Nie, D. Chalasani, D. P. Abraham, Y. Chen, A. Bose, B. L. Lucht, *J. Phys. Chem. C* **2013**, *117*, 1257–1267; b) M. Onuki, S. Kinoshita, Y. Sakata, M. Yanagidate, Y. Otake, M. Ue, M. Deguchi, *J. Electrochem. Soc.* **2008**, *155*, A794; c) G. Gachot, P. Ribière, D. Mathiron, S. Grugeon, M. Armand, J.-B. Leriche, S. Pilard, S. Laruelle, *Anal. Chem.* **2011**, *83*, 478–485; d) M. N. Richard, J. R. Dahn, *J. Electrochem. Soc.* **1999**, *146*, 2068; e) B. Michalak, B. B. Berkes, H. Sommer, T. Bergfeldt, T. Brezesinski, J. Janek, *Anal. Chem.* **2016**, *88*, 2877–2883.
[70] B. Strehle, S. Solchenbach, M. Metzger, K. U. Schwenke, H. A. Gasteiger, *J. Electrochem. Soc.* **2017**, *164*, A2513–A2526.
[71] P. Tikuisis, D. M. Kane, T. M. McLellan, F. Buick, S. M. Fairburn, *J. Appl. Physiol.* **1992**, *72*, 1311–1319.
[72] L. Xing, W. Li, C. Wang, F. Gu, M. Xu, C. Tan, J. Yi, *J. Phys. Chem. B* **2009**, *113*, 16596–16602.
[73] H. Ota, Y. Sakata, A. Inoue, S. Yamaguchi, *J. Electrochem. Soc.* **2004**, *151*, A1659.
[74] H. Yoshida, T. Fukunaga, T. Hazama, M. Terasaki, M. Mizutani, M. Yamachi, *J. Power Sources* **1997**, *68*, 311–315.
[75] C. Han, Y.-B. He, M. Liu, B. Li, Q.-H. Yang, C.-P. Wong, F. Kang, *J. Mater. Chem. A* **2017**, *5*, 6368–6381.
[76] a) N. Takami, T. Ohsaki, H. Hasebe, M. Yamamoto, *J. Electrochem. Soc.* **2002**, *149*, A9; b) H. Wang, E. Rus, T. Sakuraba, J. Kikuchi, Y. Kiya, H. D. Abruña, *Anal. Chem.* **2014**, *86*, 6197–6201; c) M. Holzapfel, A. Würsig, W. Scheifele, J. Vetter, P. Novák, *J. Power Sources* **2007**, *174*, 1156–1160; d) M. Xu, N. Tsiouvaras, A. Garsuch, H. A. Gasteiger, B. L. Lucht, *J. Phys. Chem. C* **2014**, *118*, 7363–7368; e) W. Kong, H. Li, X. Huang, L. Chen, *J. Power Sources* **2005**, *142*, 285–291.
[77] C. L. Campion, W. Li, B. L. Lucht, *J. Electrochem. Soc.* **2005**, *152*, A2327.
[78] Y.-L. Yang, S. G. Ramaswamy, W. B. Jakoby, *J. Biol. Chem.* **1998**, *273*, 7814–7817.
[79] S. E. Sloop, J. B. Kerr, K. Kinoshita, *J. Power Sources* **2003**, *119–121*, 330–337.
[80] a) A. T. S. Freiberg, J. Sicklinger, S. Solchenbach, H. A. Gasteiger, *Electrochim. Acta* **2020**, *346*, 136271; b) L. Zhang, E. A. Müller Gubler, C.-W. Tai, Ł. Kondracki, H. Sommer, P. Novák, M. El Kazzi, S. Trabesinger, *ACS Appl. Mater. Interfaces* **2022**, *14*, 13240–13249.
[81] J. K. Papp, N. Li, L. A. Kaufman, A. J. Naylor, R. Younesi, W. Tong, B. D. McCloskey, *Electrochim. Acta* **2021**, *368*, 137505.
[82] B. S. Parimalam, A. D. MacIntosh, R. Kadam, B. L. Lucht, *J. Phys. Chem. C* **2017**, *121*, 22733–22738.
[83] M. B. Smith, J. March, *March's Advanced Organic Chemistry: Reactions, Mechanisms, and Structure*, John Wiley & Sons, **2020**.
[84] J. Lamb, C. J. Orendorff, E. P. Roth, J. Langendorf, *J. Electrochem. Soc.* **2015**, *162*, A2131.
[85] a) W. M. Dose, W. Li, I. Temprano, C. A. O'Keefe, B. L. Mehdi, M. F. L. De Volder, C. P. Grey, *ACS Energy Lett.* **2022**, *7*, 3524–3530; b) B. Li, Z. Zhuo, L. Zhang, A. Iadecola, X. Gao, J. Guo, W. Yang, A. V. Morozov, A. M. Abakumov, J.-M. Tarascon, *Nat. Mater.* **2023**, *22*, 1370–1379; c) J. Lee, J. K. Papp, R. J. Clément, S. Sallis, D.-H. Kwon, T. Shi, W. Yang, B. D. McCloskey, G. Ceder, *Nat. Commun.* **2017**, *8*, 981.
[86] D. Streich, C. Erk, A. Guéguen, P. Müller, F.-F. Chesneau, E. J. Berg, *J. Phys. Chem. C* **2017**, *121*, 13481–13486.
[87] a) B. Li, G. Rousse, L. Zhang, M. Avdeev, M. Deschamps, A. M. Abakumov, J.-M. Tarascon, *Energy Environ. Sci.* **2023**, *16*, 1210–1222; b) B. Li, M. T. Sougrati, G. Rousse, A. V. Morozov, R. Dedryvère, A. Iadecola, A. Senyshyn, L. Zhang, A. M. Abakumov, M.-L. Doublet, J.-M. Tarascon, *Nat. Chem.* **2021**, *13*, 1070–1080; c) W. Yin, A. Grimaud, G. Rousse, A. M. Abakumov, A. Senyshyn, L. Zhang, S. Trabesinger, A. Iadecola, D. Foix, D. Giaume, J.-M. Tarascon, *Nat. Commun.* **2020**, *11*, 1252; d) M. Ting, M. Burigana, L. Zhang, Y. Z. Finfrock, S. Trabesinger, A. Jonderian, E. McCalla, *Chem. Mater.* **2020**, *32*, 849–857.
[88] B. Li, K. Kumar, I. Roy, A. V. Morozov, O. V. Emelyanova, L. Zhang, T. Koç, S. Belin, J. Cabana, R. Dedryvère, A. M. Abakumov, J.-M. Tarascon, *Nat. Mater.* **2022**, *21*, 1165–1174.
[89] S. E. Renfrew, B. D. McCloskey, *ACS Appl. Energ. Mater.* **2019**, *2*, 3762–3772.
[90] N. Mahne, S. E. Renfrew, B. D. McCloskey, S. A. Freunberger, *Angew. Chem. Int. Ed.* **2018**, *57*, 5529–5533.
[91] L. Manceron, L. Andrews, *J. Phys. Chem.* **1986**, *90*, 4514–4528.
[92] E. Peled, *J. Electrochem. Soc.* **1979**, *126*, 2047.
[93] J. O. Besenhard, M. W. Wagner, M. Winter, A. D. Jannakoudakis, P. D. Jannakoudakis, E. Theodoridou, *J. Power Sources* **1993**, *44*, 413–420.
[94] A. Guéguen, D. Streich, M. He, M. Mendez, F. F. Chesneau, P. Novák, E. J. Berg, *J. Electrochem. Soc.* **2016**, *163*, A1095.
[95] a) X. Zhang, L. Wang, T. Zheng, K.-H. Lam, *Batteries & Supercaps* **2023**, *6*, e202200495; b) X. Zhang, L. Wang, T. Zheng, K.-H. Lam, *Energy Fuels* **2023**, *37*, 11419–11431.
[96] B. T. Heligman, K. P. Scanlan, A. Manthiram, *J. Electrochem. Soc.* **2021**, *168*, 120544.
[97] a) T. Zheng, D. Kramer, R. Mönig, S. T. Boles, *ACS Sustainable Chem. Eng.* **2022**, *10*, 3203–3210; b) T. Zheng, J. Zhang, W. Jin, S. T. Boles, *ACS Appl. Energ. Mater.* **2023**, *6*, 1845–1852; c) J. Zhang, T. Zheng, K.-h. Lam, S. T. Boles, *Electrochim. Acta* **2023**, *456*, 142437; d) T. Zheng, J. Zhang, X. Guo, W. Jin, S. T. Boles, *Electrochim. Acta* **2024**, *485*, 144127.
[98] L. Zhang, G. Chen, E. J. Berg, J.-M. Tarascon, *Adv. Energy Mater.* **2017**, *7*, 1602200.

[99] a) J. Zhang, T. Zheng, K.-W. E Cheng, K.-h. Lam, S. T. Boles, *J. Electrochem. Soc.* **2023**, *170*, 100518; b) L. Zhang, C. Tsolakidou, S. Mariyappan, J.-M. Tarascon, S. Trabesinger, *Energy Storage Mater.* **2021**, *42*, 12–21.
[100] a) T. Bartsch, F. Strauss, T. Hatsukade, A. Schiele, A. Y. Kim, P. Hartmann, J. Janek, T. Brezesinski, *ACS Energy Lett.* **2018**, *3*, 2539–2543; b) F. Strauss, J. H. Teo, A. Schiele, T. Bartsch, T. Hatsukade, P. Hartmann, J. Janek, T. Brezesinski, *ACS Appl. Mater. Interfaces* **2020**, *12*, 20462–20468; c) C. Sångeland, B. Sun, D. Brandell, E. J. Berg, J. Mindemark, *Batteries & Supercaps* **2021**, *4*, 785–790.
[101] a) L. Zhang, X. Hou, K. Edström, E. J. Berg, *Batteries & Supercaps* **2022**, *5*, e202200336; b) M. He, K. Fic, E. Fŗckowiak, P. Novák, E. J. Berg, *Energy Environ. Sci.* **2016**, *9*, 623–633; c) Q. Duan, K. Xue, X. Yin, D. Y. W. Yu, *J. Power Sources* **2023**, *558*, 232356; d) T. Zheng, M. H. Tahmasebi, B. Li, Y. Li, S. Ran, T. S. Glen, K.-H. Lam, I.-S. Choi, S. T. Boles, *ChemElectroChem* **2018**, *5*, 2199–2207; e) J. Xie, Z. Liang, Y.-C. Lu, *Nat. Mater.* **2020**, *19*, 1006–1011; f) X. Hou, L. Zhang, N. Gogoi, K. Edström, E. J. Berg, *Small* **2023**, *20*, 2308577.
[102] L. Ma, Q. Li, Y. Ying, F. Ma, S. Chen, Y. Li, H. Huang, C. Zhi, *Adv. Mater.* **2021**, *33*, 2007406.
[103] L. W. Sommer, A. Raghavan, P. Kiesel, B. Saha, J. Schwartz, A. Lochbaum, A. Ganguli, C.-J. Bae, M. Alamgir, *J. Electrochem. Soc.* **2015**, *162*, A2664–A2669.
[104] W. Jin, Y. Cao, F. Yang, H. L. Ho, *Nat. Commun.* **2015**, *6*, 6767.
[105] C. Leitão, C. Novo, G. Yang, C. Tang, J. L. Pinto, *Latin America Optics and Photonics Conference* (Sao Sebastiao) **2012**, LS2 C.1.
[106] G. Yang, C. Leitão, Y. Li, J. Pinto, X. Jiang, *Measurement* **2013**, *46*, 3166–3172.
[107] a) M. Janzen, D. Kramer, R. Mönig, *Energy Technol.* **2021**, *9*, 2000867; b) Z. Choi, D. Kramer, R. Mönig, *J. Power Sources* **2013**, *240*, 245–251.
[108] a) T. Zheng, D. Kramer, M. H. Tahmasebi, R. Mönig, S. T. Boles, *ChemSusChem* **2020**, *13*, 5910–5920; b) A. Al-Obeidi, D. Kramer, S. T. Boles, R. Mönig, C. V. Thompson, *Appl. Phys. Lett.* **2016**, *109*, 071902.
[109] J. Hodgkinson, R. P. Tatam, *Meas. Sci. Technol.* **2012**, *24*, 012004.
[110] P. S. J. Russell, P. Hölzer, W. Chang, A. Abdolvand, J. Travers, *Nat. Photonics* **2014**, *8*, 278–286.
[111] F. Benabid, F. Couny, J. Knight, T. Birks, P. S. J. Russell, *Nature* **2005**, *434*, 488–491.
[112] a) Y. Hoo, S. Liu, H. L. Ho, W. Jin, *IEEE Photonics Technology Letters* **2010**, *22*, 296–298; b) F. Yang, W. Jin, Y. Lin, C. Wang, H. Lut, Y. Tan, *J. Lightwave Technol.* **2016**, *35*, 3413–3424.
[113] S. E. Bialkowski, N. G. Astrath, M. A. Proskurnin, *Photothermal spectroscopy methods*, John Wiley & Sons, **2019**.
[114] F. Yang, F. Gyger, L. Thévenaz, *Nat. Photonics* **2020**, *14*, 700–708.
[115] P. Zhao, Y. Zhao, H. Bao, H. L. Ho, W. Jin, S. Fan, S. Gao, Y. Wang, P. Wang, *Nat. Commun.* **2020**, *11*, 847.
[116] H. Bao, Y. Hong, W. Jin, H. L. Ho, C. Wang, S. Gao, Y. Wang, P. Wang, *Opt. Express* **2020**, *28*, 5423–5435.
[117] Y. Hong, H. Bao, W. Jin, S. Jiang, H. L. Ho, S. Gao, Y. Wang, *Sensors* **2020**, *20*, 6084.
[118] F. Liu, H. Bao, H. L. Ho, W. Jin, S. Gao, Y. Wang, *Opt. Express* **2021**, *29*, 43445–43453.
[119] F. Chen, S. Jiang, W. Jin, H. Bao, H. L. Ho, C. Wang, S. Gao, *Opt. Express* **2020**, *28*, 38115–38126.
[120] F. Chen, S. Jiang, H. L. Ho, S. Gao, Y. Wang, W. Jin, *Anal. Chem.* **2022**, *94*, 13473–13480.
[121] Y. Hong, H. Bao, F. Chen, W. Jin, H. L. Ho, S. Gao, Y. Wang, *Laser Photonics Rev.* 2300358.
[122] H. Bao, W. Jin, Y. Hong, H. L. Ho, S. Gao, Y. Wang, *J. Lightwave Technol.* **2022**, *40*, 313–322.
[123] a) N. A. David, P. M. Wild, J. Jensen, T. Navessin, N. Djilali, *J. Electrochem. Soc.* **2010**, *157*, B1173; b) T. Zheng, S. T. Boles, *ACS Omega* **2022**, *7*, 37867–37872.
[124] A. K. Farquhar, G. S. Henshaw, D. E. Williams, *ACS Sens.* **2021**, *6*, 1295–1304.
[125] T.-V. Dinh, I.-Y. Choi, Y.-S. Son, J.-C. Kim, *Sens. Actuators B* **2016**, *231*, 529–538.
[126] X. Lu, J.-M. Tarascon, J. Huang, *eTransportation* **2022**, *14*, 100207.

Manuscript received: January 23, 2024
Revised manuscript received: May 5, 2024
Version of record online: ■■, ■■

REVIEW

Gas evolution is fundamentally problematic in rechargeable batteries. This paper reviews the real-time gas sensing technologies in laboratories, shedding light on the gassing mechanisms in battery cells with various cell chemistries. Herein, a new sensing method based on fiber-enhanced laser spectroscopy is proposed, which can potentially be used in commercial batteries.

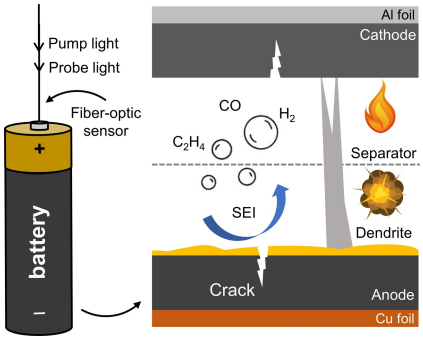

Dr. T. Zheng, Dr. M. Muneeswara, Dr. H. Bao, Ass. Prof. J. Huang, Ass. Prof. L. Zhang, Ass. Prof. D. S. Hall, Prof. S. T. Boles, Prof. W. Jin**

1 – 25

Gas Evolution in Li-ion Rechargeable Batteries: A Review on Operando Sensing Technologies, Gassing Mechanisms, and Emerging Trends